Computers and Concrete, *Vol. 17, No. 3 (2016) 353-386*
DOI: http://dx.doi.org/10.12989/cac.2016.17.3.353

Software for biaxial cyclic analysis of reinforced concrete columns

Fatemeh Shirmohammadi[*1] and Asad Esmaeily[2a]

[1]*Walter P Moore Associates, Inc., Kansas City, Missouri, USA*
[2]*Department of Civil Engineering, Kansas State University, Manhattan, Kansas, USA*

(Received October 3, 2014, Revised December 28, 2015, Accepted February 8, 2016)

Abstract. Realistic assessment of the performance of reinforced concrete structural members like columns is needed for designing new structures or maintenance of the existing structural members. This assessment requires analytical capability of employing proper material models and cyclic rules and considering various load and displacement patterns. A computer application was developed to analyze the non-linear, cyclic flexural performance of reinforced concrete structural members under various types of loading paths including non-sequential variations in axial load and bi-axial cyclic load or displacement. Different monotonic material models as well as hysteresis rules, were implemented in a fiber-based moment-curvature and in turn force-deflection analysis, using proper assumptions on curvature distribution along the member, as in plastic-hinge models. Performance of the program was verified against analytical results by others, and accuracy of the analytical process and the implemented models were evaluated in comparison to the experimental results. The computer application can be used to predict the response of a member with an arbitrary cross section and various type of lateral and longitudinal reinforcement under different combinations of loading patterns in axial and bi-axial directions. On the other hand, the application can be used to examine analytical models and methods using proper experimental data.

Keywords: reinforced concrete; cyclic behavior; force-deflection; moment-curvature; bi-axial; fiber-based, material model; computer application; windows-based

1. Introduction

Loading history, pattern, intensity, and linear combinations of loads, specifically lateral and axial loads can significantly affect the behavior of RC columns (Sadeghvaziri and Fouch 1991, Lee *et al.* 2009). During an earthquake, a majority of buildings are subject to bi-axial lateral earthquake forces and variable cyclic axial force. Bi-axial motion is induced in the columns of irregular buildings, even against one-directional earthquake motions. Experimental studies and investigations of damaged structures after earthquakes have proven that damage which is caused by bi-directional earthquake motions is different and, in most cases, more extensive than the damage caused by uni-axial earthquake motions (Marante and Flórez-López 2002, Rodrigues *et al.*

*Corresponding author, Ph.D., E-mail: fatemeh@k-state.edu
[a]Professor, E-mail: asad@k-state.edu

http://www.techno-press.org/?journal=cac&subpage=8 ISSN: 1598-8198 (Print), 1598-818X (Online)

2013).

Performance of reinforced concrete sections with arbitrary cross-section shapes has been studied by a number of researchers (Yen 1991, Yau 1993, Rodriguez and Aristizabal-Ochao 1999, Fafitis 2000, Sfakianakis 2002, Bonet *et al.* 2004, Sousa and Muniz 2007, Charalampakis 2008, Rosati *et al.* 2008, Papanikolau 2012) with an attempt to develop new methods, algorithms and small computer applications to calculate the axial force-bending moment interaction surface of a section. To construct the failure surface of a section, monotonic loading were employed in these studies; however, when exposed to a dynamic excitation such as wind, tornado, or earthquake, columns can be subjected to a combined non-proportional bi-lateral and axial directions. This is more pronounced in earthquake excitations, specifically in near-fault regions with high vertical and horizontal ground accelerations, large velocity pulses, directional effects, repetitive pulse effects, and aftershocks.

Estimation of the available force and displacement capacity, energy dissipation and the inflicted damage on a structural element or occurrence of a certain limit state with a reasonable accuracy requires a realistic prediction of the performance of a structure. Accuracy of the analytical predictions depends on the employed analytical methods and implemented material models, constitutive laws hysteresis rules, and distribution of curvature along the member. Detailed finite element analysis using available commercial software like ABAQUS or open source software like OpenSees has a steep learning curve and is not the first choice for a design engineer who prefers less sophisticated approaches.

Most of the small and user-friendly computer applications are limited to section analysis under a constant axial load and monotonic, and very few cyclic, uni-lateral displacement or force. To address the need for a simple, yet accurate analytical tool for performance assessment of reinforced concrete columns, a computer program was developed using relatively simple analytical methods and material models to predict the performance of reinforced concrete structures under various loading conditions, including cyclic lateral displacement under a non-proportionally variable axial load, with an acceptable accuracy (Esmaeily and Xiao 2005, Esmaeily and Peterman 2007); however, it was limited to circular, rectangular and hollow circular/rectangular sections, and uniaxial lateral curvature or displacement.

The computer program described in this paper is the next generation of the aforesaid program with more functionality and options. It employs both analytical and numerical solutions to assess the performance of a reinforced concrete section and member. The triangulation of the section makes it possible to have any cross sectional geometry. The bi-axial lateral curvature/displacement/force combined with any sequence of axial load provides the opportunity to analyze the performance of a reinforced concrete column under any load and displacement path. This includes cyclic bi-axial moment-curvature response of a section, under a constant, proportionally-variable, or independently-variable axial load; demanding a numerical solution where each element, here triangle, is traced in terms of its strain and stress history.Using unconventional reinforcement, such as FRP, in lateral as well as longitudinal direction is another feature added to this application.

Accuracy of various material models, hysteresis rules, and other assumptions, in simulating the behavior of a reinforced concrete member tested under a certain loading pattern can be examined by this application, using the respected experimental data.

Performance of the developed computer application has been assessed through various types of analysis for RC members compared to respected experimental data, including moment-curvature analysis of a hollow square cross section, force-deflection analysis of an oval section under axial

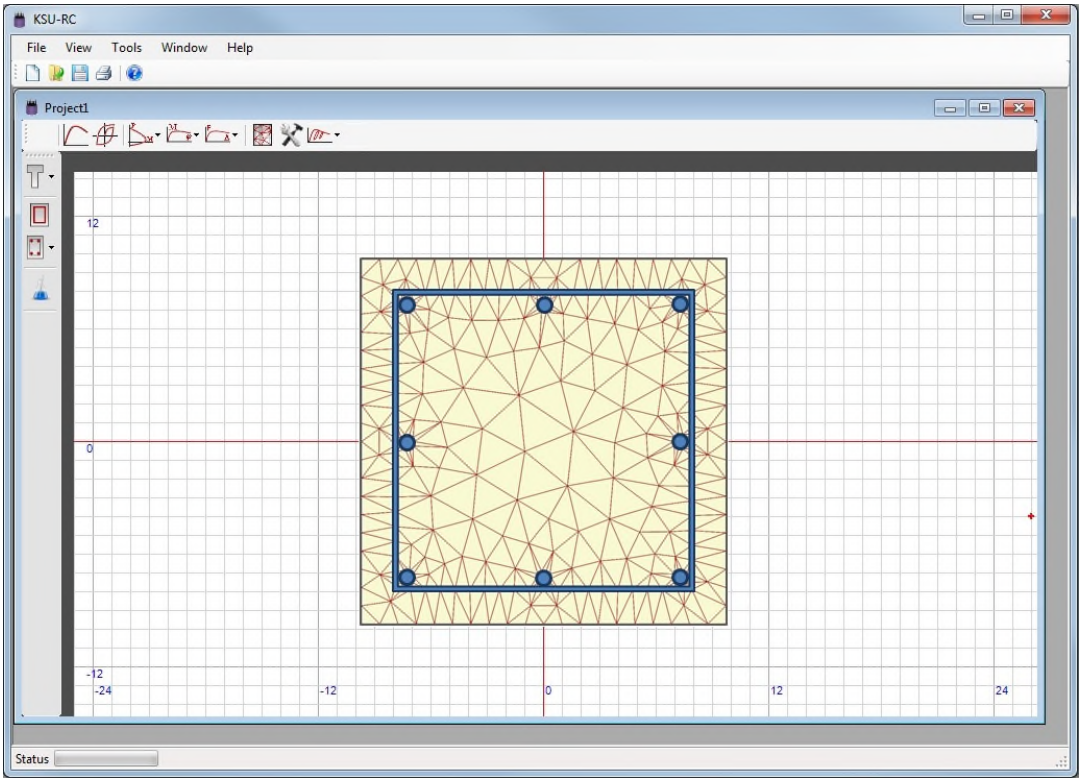

Fig. 1 Main window of the developed windows-based computer application

force and uniaxial lateral displacement and a square section under axial force and bi-axial lateral displacements, and the axial force-bending moment interaction surface for a square section.

2. Program description and assumptions

Development of a user-friendly and simple, yet accurate computer program capable of analyzing the performance of reinforced concrete columns with any cross section, reinforced by conventional or unconventional reinforcement in lateral and/or longitudinal directions under any load/displacement pattern was the main goal. The main window of this computer application is shown in Fig. 1. The load/displacement pattern can be a combination of independent biaxial curvature or moment with any axial load pattern in a moment-curvature analysis; or independent bi-axial lateral displacement or force under an independently variable axial load. The behavior of a section with an arbitrary shape under various loading scenarios has been modeled using the Bernoulli-Euler assumption in which plane sections remain plane after deformation. The arbitrary-shape section may consist of various material and reinforcement and may have any hole/opening. Constitutive material in the arbitrary-shape section may have any monotonic and cyclic behavior.

Analysis is based on fiber modeling of the section and in turn the member, as the backbone analytical method, effectively used by others (Prakash *et al.* 1993, Mazzoni *et al.* 2006).

The analysis addressed by the developed computer applications includes (i) Construction of

code-based 3D axial force-bending moment interaction surface for RC columns with conventional lateral steel reinforcement using American Concrete Institute stress-block (ACI 318-11), (ii) Construction of axial force-bending moment interaction surface using material models for the meshed RC columns laterally reinforced by steel, FRP or both steel and FRP assuming a constant strain at the extreme compressive fiber, (iii) Construction of real axial force-bending moment failure surface considering material models for the meshed RC columns laterally reinforced by steel, FRP or both steel and FRP with or without considering the axial force loading pattern (iv) Code-based biaxial moment-curvature analysis for RC columns with conventional lateral steel reinforcement considering ACI stress-block, (v) Biaxial moment-curvature analysis considering the meshed section and using proper material models with any pattern of curvature in the two lateral directions and any variation of axial load, (vi) Biaxial force-deflection analysis using proper material models and plastic hinge method, with any displacement patterns in the two lateral directions and arbitrary axial load pattern.

3. Cross-section

Fiber-based method was employed to analyze RC sections in the developed computer application. Triangular meshing is used to create cross-section fibers. In the triangulation algorithm used in the computer application, various components of a column's section are defined as separate regions. Each region is divided into a number of fibers and each fiber, depending on the material and location of the region, follows a particular cyclic rule and a monotonic material model as the envelope curve of the cyclic model. Longitudinal bars are considered separately in the model with their own monotonic and cyclic rules and load history. Since triangular meshing was employed, the cross-section of a beam-column can have an arbitrary shape with or without holes/opening. The composite section can be reinforced longitudinally by steel/FRP bars and laterally by conventional steel (tie/spiral), FRP warps or both lateral steel and FRP warps. The effect of lateral reinforcement was indirectly taken into account in modeling; since, uniaxial stress-strain behavior of the region enclosed by lateral reinforcement is affected by lateral reinforcement. FRP warps can have stiffness in axial and lateral directions, depending on the orientation of FRP fibers. The effect of FRP warps with fibers only in the hoop direction is modeled indirectly through the stress-strain relationship of concrete regions. The fiber arrangement of a composite section is shown in Fig. 2. The composite section in Fig. 2 has four regions: (i) steel or FRP bars, (ii) section core region, (iii) region between FRP warps and lateral steel reinforcement (or cover concrete for conventionally reinforced sections), and (iv) FRP wraps region. Fig. 3 shows the

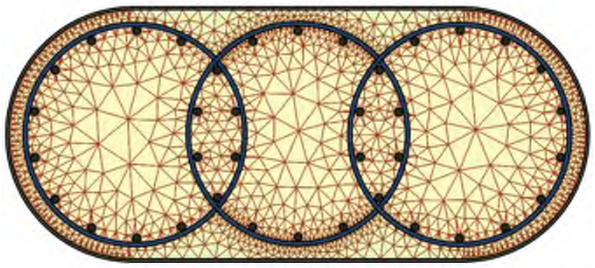

Fig. 2 Composite section

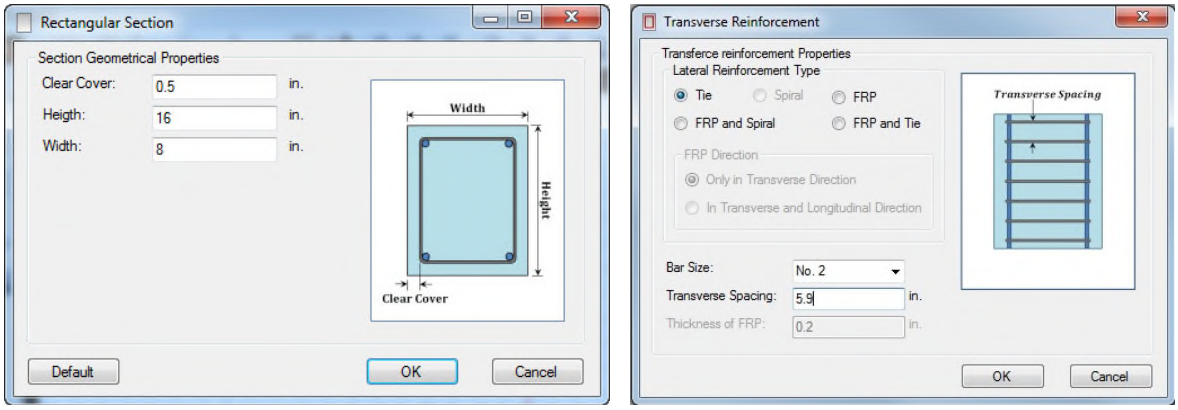

Fig. 3 Sample forms for section geometry and lateral reinforcement

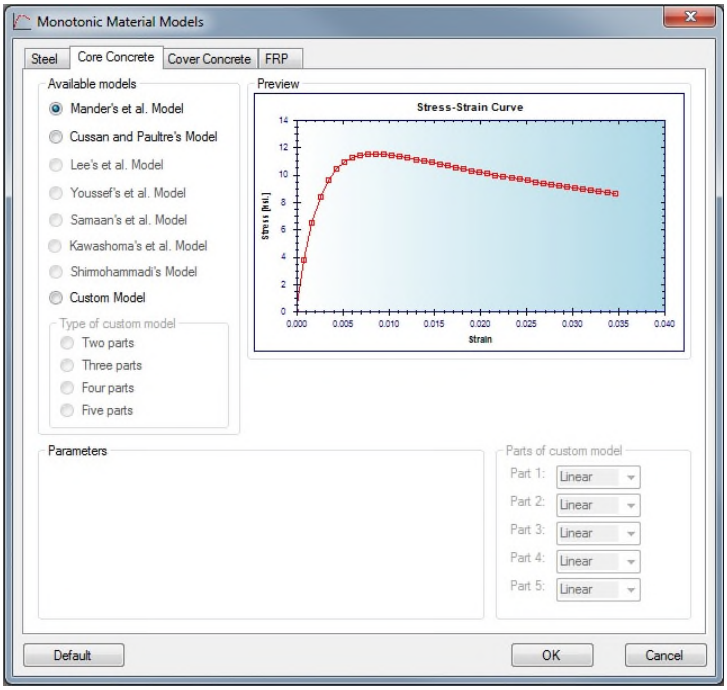

Fig. 4 Sample input forms for monotonic behavior of materials

sample forms of the developed windows-based computer application which are used to input section geometry, and lateral reinforcements.

4. Material models

4.1 Monotonic material models

To model uniaxial monotonic behavior of fibers with various materials, a number of well-

established existing material models were implemented in the computer application. Fig. 4 shows a sample form of the developed windows-based computer application which is used to specify the monotonic behavior of various materials.

For plain/unconfined concrete, the Mander *et al.* model (Mander *et al.* 1988) for low to medium strength concrete and Cusson and Paultre's model (1995) for high-strength concrete were implemented in the program. For concrete confined by steel lateral reinforcement, Mander *et al.*'s model (1988) for low to medium strength concrete and Cusson and Paultre's model (1995) for high-strength concrete were chosen because of their accuracy in predicting the behavior of circular and rectangular concrete columns with various longitudinal and lateral steel configurations.

Mander *et al.*'s model (1988) was developed analytically for circular or rectangular cross-section, under monotonic or cyclic static or dynamic loading. The RC section may have any general confinement type provided by either spiral or circular hoops, or rectangular hoops with or without supplementary cross-tie. In this model, the effect of any confinement type is taken into account by defining an effective lateral confining pressure. The effective lateral confining pressure in this model depends on configuration of the lateral and longitudinal reinforcement. To predict the strain corresponding to first fracture, Mander *et al.* used an energy balance approach by equating the strain energy which is stored in the concrete caused by confinement to the strain energy capacity of the lateral reinforcement (Mander *et al.* 1988) The stress- strain relationship of Mander *et al.*'s model is based on an equation proposed by Popovics (1973). This model has been used by many researchers to model monotonic behavior of concrete confined by conventional reinforcement. Since the proposed stress-strain models for normal-strength concrete may overestimate the strength and fracture strain of high-strength concrete, Cusson and Paultre (1995) proposed their model to predict monotonic behavior of high-strength concrete confined by steel ties, using the experimental results of 50 large-scale high-strength concrete tied columns tested under eccentric loading. The effects of tie-yield strength, concrete compressive strength, tie configuration, and lateral and longitudinal reinforcement ratios were considered by Cusson and Paultre in developing their model (Cusson and Paultre 1995) The Cusson and Paultre's stress-strain curve for confined and unconfined concrete consists of two parts: the initial part is a relationship proposed by Popovics (1973) originally and the second part is a modification of the relationship proposed by Fafitis and Shah (Fafitis and Shah 1985) for high-strength confined concrete. As reported by Cusson and Paultre (1995), the yield strength of lateral reinforcement is developed at the peak strength of concrete only for well-confined high-strength concrete specimens; therefore, the peak strength of confined concrete is computed employing an iterative process in this model.

Formulas of these two models are listed in Table 1. In the formulation of Mander *et al.* (1988) and Cusson-Paultre models (1995), the confinement effectiveness coefficient for circular and rectangular cross-section shapes is calculated using the following equations:

- For circular cross-section with tie
- For circular cross-section with spiral
- For rectangular cross-section

$$k_e = \frac{\left(1-\frac{s'}{2d_c}\right)^2}{1-\rho_{cc}}, \quad \text{For circular cross-section with tie} \tag{1}$$

$$k_e = \frac{\left(1-\frac{s'}{2d_c}\right)^2}{1-\rho_{cc}}, \quad \text{For circular cross-section with spiral}$$

$$k_e = \frac{\left(1-\sum_{i=1}^{n}\frac{\left(w_i'\right)^2}{6b_c \times d_c}\right)\times\left(1-\frac{s'}{2b_c}\right)\times\left(1-\frac{s'}{2d_c}\right)}{1-\rho_{cc}}, \quad \text{For rectangular cross-section}$$

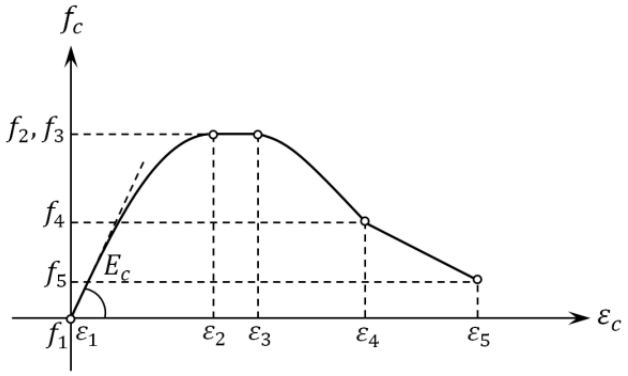

Fig. 5 Example of "Custom Model" for plain or confined concrete

Samaan *et al.* (1998) and Youssef *et al.* (2007) models were chosen as representative models for concrete confined by FRP. Samaan *et al.* developed a bilinear stress-strain model for FRP-confined concrete based on a total 30 cylindrical specimens which were tested under uniaxial compression loading (Samaan *et al.* 1998). They used a four-parameter relationship, originally proposed by Richard and Abbott (1975) to model the initial behavior of FRP-confined concrete. Calculating the fracture strain and its corresponding stress, the initial curve is followed by a line connecting the initial part to the fracture point.

Using results of an experimental program including large-scale circular, rectangular and square short columns confined by carbon-FRP and E-glass-FRP warps, Youssef *et al.* (2007) developed a stress-strain model for concrete confined by FRP. This model is applicable for predicting monotonic behavior of low to high-confined concrete. The initial relationship of this model is a polynomial function which is followed by an ascending or descending linear part, representing low and moderate to high-strength confinement, respectively.

For concrete confined by FRP and conventional lateral steel, Kawashima *et al.* (2000), Lee *et al.* (2009), and Shirmohammadi *et al.* (2014) models were implemented. Kawashima *et al.* stress-strain model developed by combining Hoshikuma *et al.* (1997) model for concrete confined by steel tie reinforcement and Hostani *et al.* (1998) model for concrete confined by carbon-FRP. The initial part of this model is a polynomial which is followed by a linear path. The linear part of this model can be ascending or descending depending on the confinement ratio of concrete section (Kawashima *et al.* 2000).

Table 1 Implemented monotonic stress-strain models for concrete confined by lateral steel

Model	Stress-Strain Curve	Maximum Stress	Strain Corresponding to Maximum Stress	Ultimate Stress	Ultimate Strain	Other Formulations
Mander *et al.* (1988)-Plain	$f_c = \frac{f_{c0}^{'} \times \frac{\varepsilon_c}{\varepsilon_{c0}} \times r}{r - 1 + \left(\frac{\varepsilon_c}{\varepsilon_{c0}}\right)^r}$	$f_{c0}^{'}$	ε_{c0}	$f_{cu} = \frac{f_{c0}^{'} \times 2 \times r}{r - 1 + 2^r}$	$2 \times \varepsilon_{c0}$	$r = \frac{E_c}{E_c - E_{sec}}$, *and* $E_{sec} = \frac{f_{c0}^{'}}{\varepsilon_{c0}}$
Cusson and Paultre (1995)-Plain	$f_c = \frac{f_{cc}^{'} \times \frac{\varepsilon_c}{\varepsilon_{c0}} \times r}{r - 1 + \left(\frac{\varepsilon_c}{\varepsilon_{c0}}\right)^r}$ *for* $\varepsilon_c \le \varepsilon_{c0}$ $f_c = f_{co}^{'} \times \exp\left(k_1 \times (\varepsilon_c - \varepsilon_{c0})^{k_2}\right)$ *for* $\varepsilon_c > \varepsilon_{cc}$	$f_{c0}^{'}$	ε_{c0}	-	-	$r = \frac{E_c}{E_c - E_{sec}}$, *and* $E_{sec} = \frac{f_{c0}^{'}}{\varepsilon_{c0}}$ $k_1 = \frac{\ln(0.5)}{(\varepsilon_{C50U} - \varepsilon_{c0})^{k_2}}$ $k_2 = 0.58$
Mander *et al.* (1988)-Confined	$f_c = \frac{f_{cc}^{'} \times \frac{\varepsilon_c}{\varepsilon_{cc}} \times r}{r - 1 + \left(\frac{\varepsilon_c}{\varepsilon_{cc}}\right)^r}$	$f_{cc}^{'} = f_{c0}^{'} \times (-1.254 + 2.254 \times \sqrt{1 + \frac{7.94 \times f_l^{'}}{f_{c0}^{'}}} - 2\frac{f_l^{'}}{f_{c0}^{'}})$	$\varepsilon_{cc} = \varepsilon_{c0} \times \left[1 + 5 \times \left(\frac{f_{cc}^{'}}{f_{c0}^{'}} - 1\right)\right]$	$f_{cu} = \frac{f_{cc}^{'} \times \frac{\varepsilon_{cu}}{\varepsilon_{cc}} \times r}{r - 1 + \left(\frac{\varepsilon_{cu}}{\varepsilon_{cc}}\right)^r}$	$110 \times \rho_s = \int_0^{\varepsilon_{cu}} f_c \, d\varepsilon_c + \int_0^{\varepsilon_{cu}} f_{sl} \, d\varepsilon_c -$ $0.017 \times \sqrt{f_{c0}^{'}}\ [MJ/m^3]$	$r = \frac{E_c}{E_c - E_{sec}}$, *and* $E_{sec} = \frac{f_{cc}^{'}}{\varepsilon_{cc}}$ $\rho_s = \frac{4A_{sp}}{d_s \times s}$ $f_l^{'} = \frac{1}{2}\rho_s \times f_{yh} \times k_e$
Cusson and Paultre (1995)-confined	$f_c = \frac{f_{cc}^{'} \times \frac{\varepsilon_c}{\varepsilon_{cc}} \times r}{r - 1 + \left(\frac{\varepsilon_c}{\varepsilon_{cc}}\right)^r}$ *for* $\varepsilon_c \le \varepsilon_{cc}$ $f_c = f_{cc}^{'} \times \exp\left(k_1 \times (\varepsilon_c - \varepsilon_{cc})^{k_2}\right)$ *for* $\varepsilon_c > \varepsilon_{cc}$	$f_{cc}^{'} = f_{c0}^{'} \times (-1.254 + 2.254 \times \sqrt{1 + \frac{7.94 \times f_l^{'}}{f_{c0}^{'}}} - 2\frac{f_l^{'}}{f_{c0}^{'}})$	$\varepsilon_{cc} = \varepsilon_{c0} + 0.21\left(\frac{f_{le}^{'}}{f_{c0}^{'}}\right)^{1.7}$	-	-	$r = \frac{E_c}{E_c - E_{sec}}$, *and* $E_{sec} = \frac{f_{cc}^{'}}{\varepsilon_{cc}}$ $k_1 = \frac{\ln(0.5)}{(\varepsilon_{C50C} - \varepsilon_{cc})^{k_2}}$ $k_2 = 0.58 + 16\left(f_{le}/f_{c0}^{'}\right)^{1.4}$ $\varepsilon_{C50C} = \varepsilon_{C50U} + 0.15\left(\frac{f_{le}^{'}}{f_{c0}^{'}}\right)^{1.1}$ $f_{le}^{'} = k_e \times \frac{f_{hcc}}{s} \times \left(\frac{A_{shx} + A_{shy}}{c_x + c_y}\right)$

Table 2 Implemented monotonic stress-strain models for concrete confined by FRP or FRP and lateral steel

Model	Stress-Strain Curve	Ultimate stress	Ultimate Strain	Other formulations
Samaan *et al.* (1998)	$f_c = \frac{(E_1 - E_2)\times\varepsilon_c}{\left[1+\left(\frac{(E_1-E_2)\times\varepsilon_c}{f_0}\right)^n\right]^{1/n}} + E_2\times\varepsilon_c$	$f'_{cu} = f'_{c0} + 6.0\times f_{lf}^{0.7}[MPa]$ $f'_{cu} = f'_{c0} + 3.38\times f_{lf}^{0.7}[ksi]$	$\varepsilon_{cu} = \frac{f'_{cu} - f_0}{E_2}$	$E_1 = 3950\sqrt{f'_{c0}}[MPa] = 47.586\sqrt{1000\times f'_{c0}}[ksi]$ $E_2 = 245.61\times f'^{0.2}_{c0} + 1.3456\times\frac{E_{frp}\times t}{d}[MPa]$ $E_2 = 52.411\times f'^{0.2}_{c0} + 1.3456\times\frac{E_{frp}\times t}{d}[ksi]$ $f_0 = 0.872\times f'_{c0} + 0.371\times f_{lf} + 6.258[MPa]$ $f_0 = 0.872\times f'_{c0} + 0.371\times f_{lf} + 0.908[ksi]$
Kawashima *et al.* (2001)	$f_c = E_c\times\varepsilon_c\left[1-\frac{1}{n}\left(1-\frac{E_2}{E_c}\right)\times\left(\frac{\varepsilon_c}{\varepsilon_t}\right)^{n-1}\right]$ *and* $n = \frac{(E_c - E_2)\times\varepsilon_t}{E_c\times\varepsilon_t - f_t}\quad 0\le\varepsilon_c\le\varepsilon_t$ *and* $E_2 > 0$ $f_c = E_c\times\varepsilon_c\left[1-\frac{1}{n}\left(\frac{\varepsilon_c}{\varepsilon_t}\right)^{n-1}\right]$ *and* $n = \frac{E_c\times\varepsilon_t}{E_c\times\varepsilon_t - f_t}\quad 0\le\varepsilon_c\le\varepsilon_t$ *and* $E_2 < 0$ $f_c = f_t + E_2\times(\varepsilon_c - \varepsilon_t)\quad \varepsilon_t\le\varepsilon_c\le\varepsilon_{cu}$	-	$\varepsilon_{cu} = 0.00383 + 0.1014\times\left(\frac{4\times t\times f_{yf}}{d_c\times f'_{c0}}\right)^{0.75}\times\left(\frac{f_{yf}}{E_{frp}}\right)^{0.5}$	$E_2 = -0.658\frac{f'^2_{c0}}{\frac{4t}{d_c}\times\varepsilon_{frp}\times E_{frp} + 0.196\times f_{ls}} + 0.078\times E_{frp}\times\sqrt{\frac{4t}{d_c}}$ $f_t = f'_{c0} + 1.93\times\frac{4t}{d_c}\times\varepsilon_{frp}\times E_{frp} + 4.4\times f_{ls}$ $\varepsilon_t = 0.003 + 0.1169\times\left(\frac{4\times t\times E_{frp}\times\varepsilon_{frp}}{d_c\times f'_{c0}}\right) + 0.0214\left(\frac{f_{ls}}{f'_{c0}}\right)$
Youssef *et al.* (2007)	$f_c = E_c\times\varepsilon_c\left[1-\frac{1}{n}\left(1-\frac{E_2}{E_c}\right)\times\left(\frac{\varepsilon_c}{\varepsilon_t}\right)^{n-1}\right]$ *and* $n = \frac{(E_c - E_2)\times\varepsilon_t}{E_c\times\varepsilon_t - f_t}\quad 0\le\varepsilon_c\le\varepsilon_t$ *and* $E_2 > 0$ $f_c = E_c\times\varepsilon_c\left[1-\frac{1}{n}\left(\frac{\varepsilon_c}{\varepsilon_t}\right)^{n-1}\right]$ *and* $n = \frac{E_c\times\varepsilon_t}{E_c\times\varepsilon_t - f_t}\quad 0\le\varepsilon_c\le\varepsilon_t$ *and* $E_2 < 0$ $f_c = f_t + E_2\times(\varepsilon_c - \varepsilon_t)\quad \varepsilon_t\le\varepsilon_c\le\varepsilon_{cu}$	$\frac{f'_{cu}}{f'_{c0}} = 1.0 + 2.25\left(\frac{f_{lf}}{f'_{c0}}\right)$	$\varepsilon_{cu} = 0.003368 + 0.259\times\left(\frac{f_{lf}}{f'_{c0}}\right)\times\left(\frac{f_{yf}}{E_{frp}}\right)^{0.5}$	$\frac{f_t}{f'_{c0}} = 1.0 + 3.0\left(\frac{4\times t\times E_{frp}\times\varepsilon_{jt}}{d\times f'_{c0}}\right)^{5/4}$ $\varepsilon_t = 0.002748 + 0.1169\times\left(\frac{4\times t\times E_{frp}\times\varepsilon_{jt}}{d\times f'_{c0}}\right)^{6/7}\times\left(\frac{f_{yf}}{E_{frp}}\right)^{0.5}$ $E_2 = \frac{f'_{cu} - f_t}{\varepsilon_{cu} - \varepsilon_t}$

Table 2 Continued

Lee *et al.* (2009)	$f_c = E_c \times \varepsilon_c + (f_{c0}^{'} - E_c \times \varepsilon_{c0}) \times \left(\frac{\varepsilon_c}{\varepsilon_{c0}}\right)^2$ $0 \le \varepsilon_c \le \varepsilon_{c0}$ $f_c = f_{c0}^{'} + (f_{cs} - f_{c0}^{'}) \times \left(\frac{\varepsilon_c - \varepsilon_{c0}}{\varepsilon_{cs} - \varepsilon_{c0}}\right)^{0.7}$ $\varepsilon_{c0} \le \varepsilon_c \le \varepsilon_{cs}$ $f_c = f_{cs} + (f_{cu}^{'} - f_{cs}) \times \left(\frac{\varepsilon_c - \varepsilon_{cs}}{\varepsilon_{cu} - \varepsilon_{cs}}\right)^{0.7}$ $\varepsilon_{cs} \le \varepsilon_c \le \varepsilon_{cu}$	$f_{cu}^{'} = f_{c0}^{'} \times \left(1 + 2\frac{f_{lf} + f_{ls}}{f_{c0}^{'}}\right)$	$\varepsilon_{cu} = \varepsilon_{c0} \times \left(1.75 + 5.25\left(\frac{f_{lf} + k_s \times f_{ls}}{f_{c0}^{'}}\right) \times \left(\frac{\varepsilon_{frp}}{\varepsilon_{c0}}\right)^{0.45}\right)$	$\varepsilon_{cs} = \varepsilon_{cu}\left\{0.85 + 0.03 \times \left(\frac{f_{lf}}{f_{ls}}\right)\right\}$ *for* $f_{lf} \ge f_{ls}$ $f_{cs} = 0.95 \times f_{cu}^{'}$ *for* $f_{lf} \ge f_{ls}$ $\varepsilon_{cs} = 0.7 \times \varepsilon_{cu}$ *and* $f_{cs} = f_{cu}^{'} \times \left(\frac{\varepsilon_{cs}}{\varepsilon_{cu}}\right)^{0.4}$ *for* $f_{lf} < f_{ls}$
Shirmohammadi *et al.* (2014)	$\frac{f_c}{f_{cu}^{'}} = \frac{n.(\varepsilon_c / \varepsilon_{cu})}{(n - 1 + (\varepsilon_c / \varepsilon_{cu}))^{nk}}$	$\frac{f_{cu}^{'}}{f_{c0}^{'}} = 1.1 + 2.5\left(\frac{f_{lf}}{f_{c0}^{'}}\right)^{0.8} \times \left(\frac{f_{ls}}{f_{c0}^{'}}\right) + 3.5\left(\frac{f_{ls}}{f_{c0}^{'}}\right)^{0.2}\left(\frac{d_c^2}{d^2}\right)^4$	$\frac{\varepsilon_{cu}}{\varepsilon_{c0}} = 2.0 + 6.5 \times \left(\frac{f_{lf}}{f_{c0}^{'}}\right)^{0.7} \times \left(\frac{f_{ls}}{f_{c0}^{'}}\right)^{0.7} + 6.0 \times \left(\frac{f_{ls}}{f_{c0}^{'}}\right)^{0.04}\left(\frac{s}{0.5 \times d}\right)^{-0.8} \times \left(\frac{E_{frp}}{f_c^{'}}\right)^{0.5}$	$n = E_c / (E_c - f_{cu}^{'} / \varepsilon_{cu})$

Lee *et al.* (2009) presented a comprehensive stress-strain model for concrete confined internally by lateral steel and externally by FRP wraps based on experimental results of total 24 concrete cylinders subjected to compression. Lee *et al.*'s model consists of three polynomials: a second-order polynomial function which is followed by another polynomial at strain corresponding to plain concrete strength, the second polynomial is followed by another polynomial at the point representing the lateral steel yield point (Lee *et al.* 2009). To estimate the ultimate stress and its corresponding strain, the Lam and Teng (Lam and Teng 2003) equations were modified by introducing two new parameters based on Lee *et al.*'s experimental results. Shirmohammadi *et al.* developed a constitutive stress-strain relationship to model the behavior of concrete confined by both FRP and lateral steel. They used Thorenfeldt *et al.* (1987) stress-strain relationship which is the modified version of Popovics (1973) equation. Using experimental data, they proposed two equations for ultimate strain and its corresponding stress for FRP and steel confined concrete. In Table 2, formulations of monotonic stress-strain models for concrete confined by FRP or FRP and conventional lateral steel are listed.

Concrete tensile strength can be considered assuming a linear equation with a slope equal to modulus of elasticity of plain concrete in all aforementioned monotonic models. In addition to aforesaid models, a custom model option was added to the program. Using "Custom Model" functionality, users can implement and use their own model, including linear and second-order polynomial segments for various regions of cross-section. "Custom Model" may include up to five segments and each segment may be linear or polynomial. An example of a Custom Model for plain or confined concrete by steel is shown in Fig. 5. This monotonic model consists of four segments; the first and third segments are polynomial, and the second and last segments are linear.

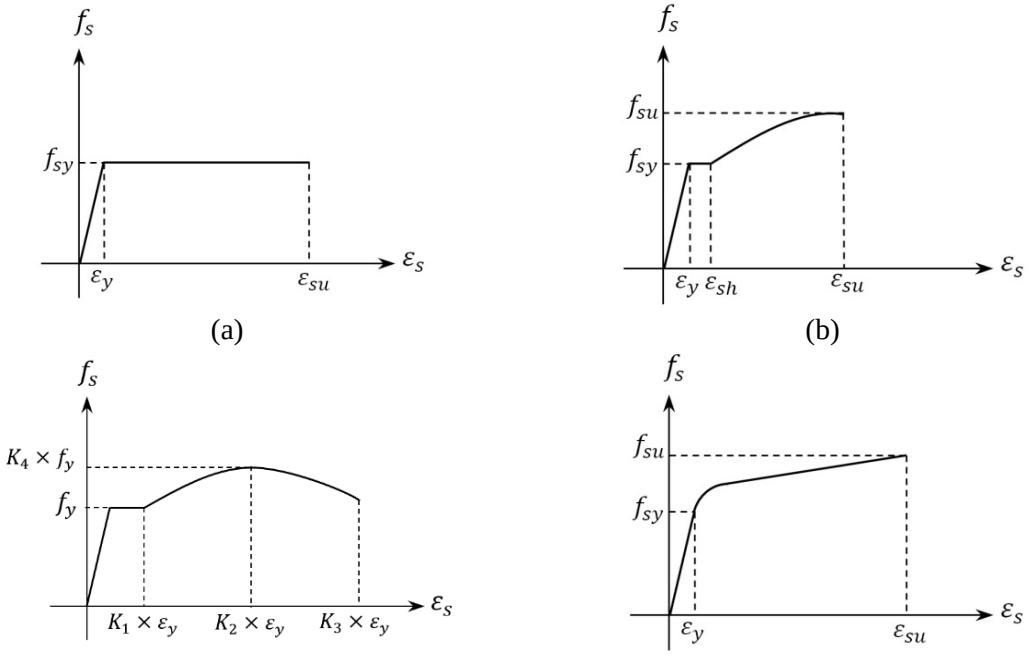

Fig. 6 Implemented steel stress-strain models in computer application: (a) Elastic-perfectly plastic model, (b) Mander *et al.* model (1984), (c) Esmaeily-Xiao model (2005), and (d) Menegotto-Pinto model (1973)

For steel, plastic-perfectly plastic model, Mander *et al.* model (1984), Esmaeily-Xiao's model (2005), and Menegotto-Pinto's model (1973) were implemented in the computer application. Fig. 6 shows these four steel monotonic models. When no information about the reinforcing steel is available except yield strength and modulus of elasticity, the plastic-perfectly plastic stress-strain model can be used for monotonic behavior of longitudinal steel bars. Esmaeily and Xiao's steel monotonic model can be employed to model behavior of longitudinal reinforcement when additional detailed information about reinforcing steel is available. Using four parameters (K_1, K_2, K_3 and K_4), the stress-strain behavior of different type of steel can be simulated. These four parameters are shown in Fig. 6. The yield plateau, strain hardening and softening of steel material are taken into account in this model (Esmaeily and Xiao 2005, Esmaeily and Shirmohammadi 2014). Having steel yield strength and modulus of elasticity, when no other information is available, the hardening and softening branch of steel monotonic model can be estimated using proposed coefficients by Esmaeily and Xiao (2002). Based on tensile experiments of steel bars, Esmaeily and Xiao proposed the ultimate strain (ε_{su}) and strength (f_{su}) for steel to be equal to 24.9 $\times$ ε_{sy} and 1.3$\times f_{sy}$, respectively (Esmaeily and Xiao 2002).

Mander *et al.*'s model (1984) was developed as a result of a wide range of tension and compression tests. This model takes into account the elastic behavior, yield plateau and strain hardening of steel material. Menegotto-Pinto's model (1973) includes a bilinear curve, the initial line has the slope of steel modulus of elasticity up to yield strength, modeling the elastic behavior of steel material, and the post-yield strength is defined as linear function with a slope equal to a portion (define by parameter) of the initial part's slope. The yield plateau characterization is neglected in Menegotto-Pinto monotonic model.

To model uniaxial behavior of FRP, a bi-linear model was used in the computer application. The slope of tensile and the slope of compressive branches are equal to tensile modulus and compressive modulus of elasticity of FRP wraps, respectively.

4.2 Cyclic material models

To model the cyclic behavior of materials in a composite section, various cyclic models were implemented in the computer application. Cyclic behavior of plain concrete can be modeled using a linear model with a slope equal to the modulus of elasticity of concrete, or models developed by Mander *et al.* (1984) and Esmaeily and Xiao (2005). For the cyclic behavior of concrete confined by conventional lateral steel, Mander *et al.* and Esmaeily-Xiao cyclic rules were implemented in the developed computer application (Fig. 7). All these cyclic models can work with any monotonic model as an envelope curve. In Mander *et al.* cyclic model the unloading path follows a concave-upward parabolic path with a zero-slope at the strain-axis. The tensile strength of concrete can be taken into account considering a linear path with a slope of plain concrete modulus of elasticity. Increasing strain, stress remains zero up to the last strain corresponding to the zero stress and after that strain will grow in a linear reloading path with a slope equal to plain concrete modulus of elasticity in the strain-axis (Mander *et al.* 1984). In Esmaeily-Xiao cyclic model the unloading path follows a parabolic path, which is concave-upward and has a slope of on the envelope curve (monotonic curve). This model may account for the tensile strength of concrete. Decreasing strain at unloading path, the stress decreases to zero and after that if the tensile strength is ignored, stress remains zero; otherwise, the stress will decrease to the tensile strength using a linear function with a slop of . Increasing strain, the stress remains zero up to the latest strain corresponding to the zero stress and then stress will increase following a concave-downward parabolic with a slope of at the

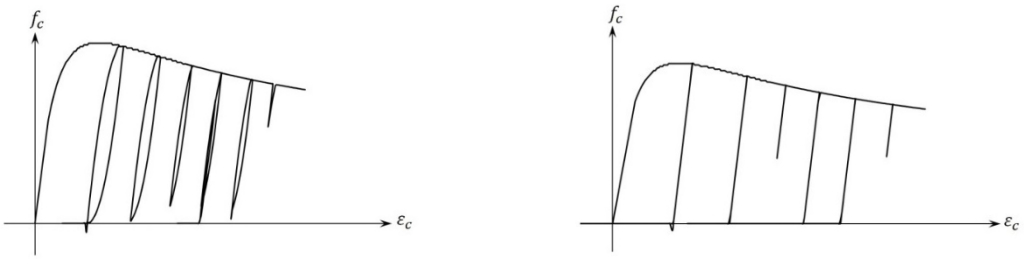

(a) (b)

Fig. 7 Implemented confined concrete cyclic models: (a) Esmaeily-Xiao model, (b) linear model

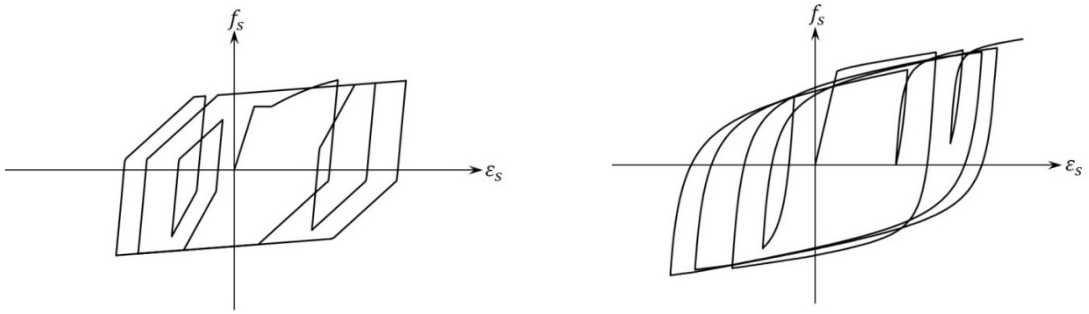

(a) (b)

Fig. 8 Implemented steel cyclic models: (a) Esmaeily-Xiao model, (b) Menegotto-Pinto model

strain-axis (Esmaeily and Xiao 2005). Cyclic behavior of concrete confined by FRP or both lateral steel and FRP can be modeled by a linear cyclic model with a slope equal to the modulus of elasticity of plain concrete. Mander *et al.* (1984) and Esmaeily-Xiao (2005) cyclic models were developed originally to model the cyclic behavior of concrete confined by lateral steel; however, they can also be applied to model the cyclic behavior of concrete confined by FRP or both FRP and lateral steel. The Esmaeily-Xiao and linear cyclic models for confined concrete are shown in Fig. 7. In this figure, the Mander *et al.* confined concrete monotonic model (Mander *et al.* 1988) is used as the envelope curve.

For steel, a linear model with a slope equal to the modulus of elasticity of steel, Menegotto-Pinto's model (1973), and Esmaeily-Xiao's model (2005) were implemented. The Menegotto-Pinto's model has a bilinear backbone curve as explained earlier. The cyclic response of steel material was defined using a non-linear equation. The shape of unloading and reloading curves are defined by three parameters R_0,a_1, and a_2. Because of numerical stability of this model and its realistic predictions, this model has been used by many researchers as a base to propose new models for steel material.

Esmaeily-Xiao hysteretic model for steel is a multi-linear model. At the reversal point, the unloading path is a linear function with a slope equal to modulus of elasticity of steel material. The Bauschinger effect is taken into account in this model by changing the slope of first unloading part into a portion of steel's modulus of elasticity beyond a certain stress (Esmaeily and Xiao 2005). To simulate the cyclic behavior of steel material in a more realistic way, this ratio and the strain at which the slope changing occurs are different in the second (tensile strain and compressive stress) and fourth (compressive strain and tensile stress) quarters from their values in the first (tensile

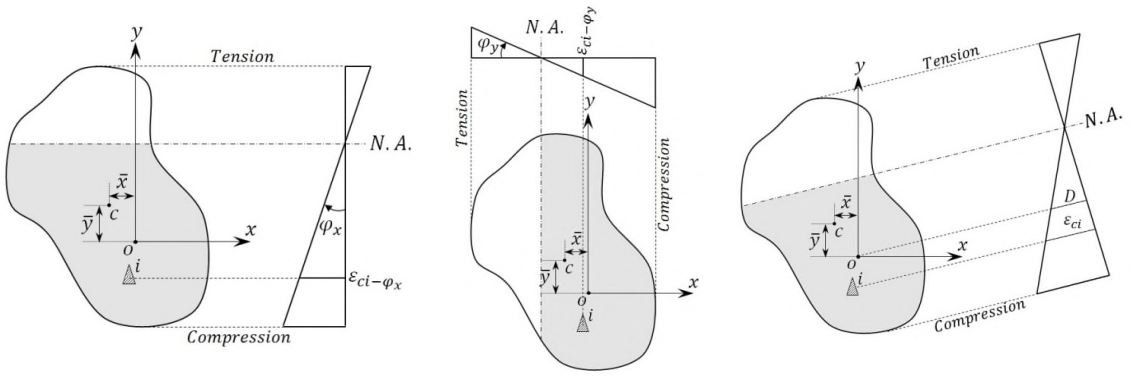

(a) (b) (c)

Fig. 9 Calculation of fiber's strain under bi-axial bending

strain and stress) and third (compressive strain and stress) quarters. Using five ratios (P_1, P_2, P_3, R_1 and R_2) in Esmaeily-Xiao's model, the hysteretic behavior of steel material can be changed. Unlike Menegotto-Pinto model, linear and Esmaeily-Xiao cyclic models can be used in conjunction with any steel monotonic model as an envelope curve. Fig. 8 shows the Esmaeily and Menegotto-Pinto cyclic models for steel material. In Fig. 8(a), Esmaeily-Xiao monotonic model was used as envelope curve of Esmaeily-Xiao cyclic model. The Menegotto-Pinto cyclic model was used in conjunction with Menegotto-Pinto monotonic model in Fig. 8(b).

5. Analysis

Since shear deformation is not modeled in the computer application, beam-column specimens should not be shear-critical. A beam column specimen is modeled as cantilever considering fix support at the column-footing interface. Axial force and lateral forces/displacements are assigned to the top of column. The centroid of a composite section is calculated with respect to a global x- and y-axis considered in the program. Considering curvature in x- and y-direction, uniaxial strain of fibers is calculated using the following equations

$$\begin{aligned} \varepsilon_{si} &= \varphi_x \times y_{si} - \varphi_y \times x_{si} - D \\ \varepsilon_{ci} &= -(\varphi_x \times y_{ci} - \varphi_y \times x_{ci} - D) \\ \varepsilon_{fi} &= \varphi_x \times y_{fi} - \varphi_y \times x_{fi} - D \end{aligned} \tag{2}$$

In the above equations, ε_{si}, ε_{ci} and ε_{fi} are uniaxial strain at steel bar, concrete fiber, and FRP fiber, respectively. x_i, y_i, φ_x and φ_y are the location of ith fiber with respect to x- and y-axis of global coordinate system, respectively, and is strain at the global coordinate's centroid (Fig. 9).

When strains of all concrete and FRP fibers and longitudinal bars are calculated, stress of fibers and bars are calculated through cyclic and monotonic models defined for each fiber or bar as follows

$$\sigma_{si} = \textit{Steel Cyclic Model}(\textit{Steel Monotonic Model}, \varepsilon_{si}, \varepsilon_{si}^{p}, \sigma_{si}^{p}, \varepsilon_{un}, \sigma_{un})$$

$$\begin{aligned} \sigma_{ci} &= Concrete\ Cyclic\ Model(Concrete\ Monotonic\ Model, \varepsilon_{ci}, \varepsilon_{ci}^{p}, \sigma_{ci}^{p}, \varepsilon_{un}, \sigma_{un}, \varepsilon_{RO}, \sigma_{RO}) \\ \sigma_{fi} &= FRP\ Cyclic\ Model(FRP\ Monotonic\ Model, \varepsilon_{fi}, \varepsilon_{fi}^{p}, \sigma_{fi}^{p}) \end{aligned} \tag{3}$$

where σ_{si}, σ_{ci} and σ_{fi} are stresses in ith steel/FRP bar, concrete fiber, and FRP fiber, respectively. Stress in each fiber depends on the current strain (ε_i), previous strain and stress of that fiber ($\varepsilon_i^p, \sigma_i^p$), strain and stress of the last point reached on the monotonic model (ε_{un}, σ_{un}) and in concrete fibers, also strain and stress of the last point reached in the unloading branch ($\varepsilon_{RO}, \sigma_{RO}$).

When the axial force and bending moments have stresses of all fibers and bars, the axial force and bending moments are calculated using the following equations

$$P = \iint_A \sigma \; dxdy = \int_A \sigma \; dA \tag{4}$$

$$\begin{aligned} M_x &= \int_A \sigma \times (y - \bar{y}) \; dA \\ M_y &= \int_A \sigma \times (x - \bar{x}) \; dA \end{aligned} \tag{5}$$

Using discrete fibers, the above equations can be written in the following discrete format

$$P = \sum_{i=1}^{n_s} A_{si} \times \sigma_{si} + \sum_{i=1}^{n_c} A_{ci} \times \sigma_{ci} + \sum_{i=1}^{n_f} A_{fi} \times \sigma_{fi}$$

$$M_x = \sum_{i=1}^{n_s} A_{si} \times \sigma_{si} \times (y_{si} - \bar{y}) + \sum_{i=1}^{n_c} A_{ci} \times \sigma_{ci} \times (y_{ci} - \bar{y}) + \sum_{i=1}^{n_f} A_{fi} \times \sigma_{fi} \times (y_{fi} - \bar{y}) \tag{6}$$

$$M_y = \sum_{i=1}^{n_s} A_{si} \times \sigma_{si} \times (x_{si} - \bar{x}) + \sum_{i=1}^{n_c} A_{ci} \times \sigma_{ci} \times (x_{ci} - \bar{x}) + \sum_{i=1}^{n_f} A_{fi} \times \sigma_{fi} \times (x_{fi} - \bar{x})$$

In the above equations, A_{si}, A_{ci} and A_{fi} are the area of ith steel/FRP bar, ith concrete fiber, and ith FRP fiber, respectively. $\bar{x}$ and $\bar{y}$ are the distance of the cross-section of beam-column specimen centroid along x- and y-direction, respectively.

5.1 Moment-curvature analysis

Monotonic moment-curvature analysis was performed with consideration of the code-based method and material models in the developed computer application. Code-based monotonic moment-curvature analysis can be conducted for RC beam-columns laterally reinforced by conventional lateral steel and longitudinally reinforced by steel bars only. However, exact monotonic and cyclic moment-curvature analysis considering material models can be performed for concrete beam-columns with any longitudinal and lateral reinforcement.

In code-based moment-curvature analysis, the “ACI stress-block” is used without considering the confinement effect. In this analysis, the angle of neutral axis respect to x-axis should be given to the computer application. The approximate code-based moment-curvature graph contains four

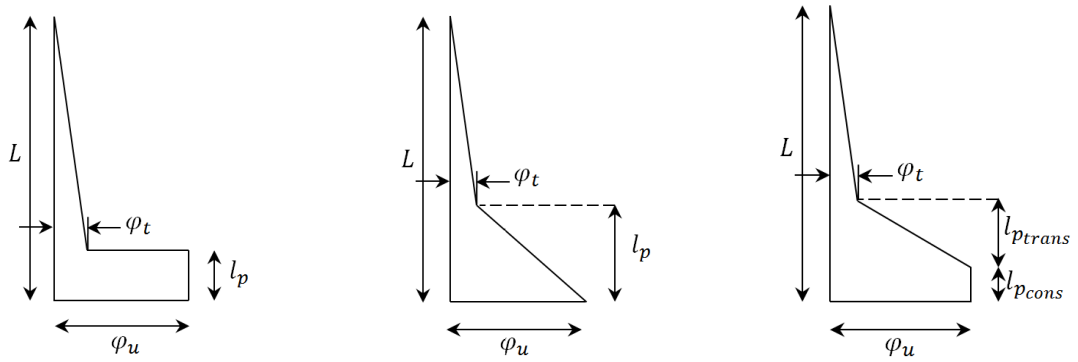

(a) (b) (c)

Fig. 10 Curvature distributing along column height as assumed in (a) Priestley and Park and Priestley and Park revised by Xiao's methods, (b) Esmaeily first method, and (c) Esmaeily second method

Table 3 Implemented plastic hinge methods in the computer application

Method	Plastic Hinge Length
Priestely and Park (1987)	$l_p = 0.08 \times L + \xi \times f_{sy} \times d$, $\xi = 0.022\ mm\,(0.15\ in.)$
Priestley and Park Revised by Xiao (Esmaeily and Xiao 2002)	$l_p = 0.08 \times L + \xi \times \sigma_s \times d$, $\xi = 0.022\ mm\,(0.15\ in.)$
Esmaeily First Method (Esmaeily and Xiao 2002)	$l_p = L \times \left(1 - \frac{M_{yield}}{M_u}\right)$, $\varphi_t = \varphi_{yield} \times \left(\frac{M_u}{M_{yield}}\right) \times \frac{\left(L - l_p\right)}{L}$
Esmaeily Second Method (Esmaeily and Peterman 2007)	$l_p = l_{pcons} + l_{p_{trans}}$, $l_{p_{cons}} = l_{p_1} + l_{p_2}$, $l_{p1} = \begin{cases} D & L/D \le 12.5 \\ 0.08 \times L & L/D > 12.5 \end{cases}$ $l_{p_2} = \xi \times \sigma_s \times d$, $\xi = 0.022\ mm\,(0.15\ in.)$ $l_{p_{trans}} = L - \frac{M_{yield}}{M_u} \times \left(L + l_{p_2}\right) - l_{p_1}$

essential points. The first point is related to the starting point of which curvature and moment are equal to zero. The second point is related to the "First Crack." For a displacement control analysis, when the curvature is changed step-by-step and moment is calculated, the bending moment drops once a crack develops. Therefore, at the same curvature (φ_{cr}), two moments are present: the moment before ($M_{cr\text{-}before}$) and the moment right after the crack ($M_{cr\text{-}before}$). For a force-controlled analysis, when curvature related to a given moment is calculated at the first crack point, the curvature jumps to a new curvature right after the first crack. Therefore, two curvatures are present: one before and one after the first crack. The third point of the code-based moment-curvature graph is related to "Steel Yield." At this point, the steel bars initially yield. The last point is related to "Ultimate Strength," considering the code-based ultimate strength of an RC section.

In moment-curvature analysis using material models, the curvature-path along x- and y-axis is known and the ultimate bending moment along x- and y-axis are calculated using material models.

Having and in each step during an iterative process, the value of *D* is calculated to set axial force equal to the applied axial force at the top of the beam-column specimen. Next, bending moments along the x- and y-axis are calculated using Eq.(6). Unlike code-based moment-curvature analysis, monotonic and also cyclic moment-curvature analysis using material models can be performed by the developed computer application.

5.2 Force-deflection analysis

To calculate flexural deformation of an RC beam-column, two methods can be employed. In the first method, flexural deformation analysis of an RC beam-column specimen is conducted using the finite element approach. This approach has high computational demands, even for the fiber element method. In Finite Element Method (FEM), the method of displacement approximation has a definitive role in the accuracy of force-deflection results. When the curvature of the critical section (at the bottom of the beam-column specimen) falls into the descending branch of the moment-curvature curve, the corresponding stiffness matrix becomes negative definite and adaptive methods (resorting trial-error) must be employed to capture force-deflection results (Esmaeily and Xiao 2002).

In the second approach, the plastic hinge concept of the critical section (or transition area) and a proper curvature distribution along the beam-column specimen height is employed to solve the force-deflection problem when curvature falls into the descending branch of the moment-curvature curve. In plastic hinge approach, column height is divided into two elastic and plastic elements. The length of the transition area (plastic hinge length), depending on the curvature distribution method, may or may not change during force-deflection analysis. Total displacement at the top of a column is a summation of elastic and plastic deformation caused by elastic and plastic elements, respectively.

In the developed computer application, the second approach was employed to perform force-deflection analysis of an RC beam-column under constant or variable axial force and cyclic or monotonic lateral forces/displacements. Nearly 30 plastic hinge models are available in the litreture, of which Priestley and Park's method (Prietley and Park 1987), Esmaeily's first and second method and Xiao's method (Esmaeily and Xiao 2002) were implemented into the windows-based computer program. Although majority of existing plastic hinge models in the literature were developed considering uniaxial behavior of RC columns, the experimental evidences confirm that plastic hinge length is not affected by bi-axial loading (Rodrigues *et al.* 2013); therefore, they are applicable even for biaxial force-deflection analysis. Priestley and Park's plastic hinge length depends on column height, longitudinal steel yield strength and rebar diameter. The curvature distribution was considered to be uniform along plastic hinge length. The axial force effect was not taken into account in this method. Later Priestly and Park plastic hinge length was modified by Xiao (Esmaeily and Xiao 2002). In the modified version, the maximum tensile stress at longitudinal bars is employed instead of steel yield strength. These plastic hinge models work well for RC columns under constant axial force and monotonic lateral force/displacement.

Esmaeily's first plastic hinge method considered a linear distribution along transition zone or plastic hinge length. The plastic hinge length applied in this model depends of yield moment and moment at critical section at each step of loading. Therefore, axial force effect and cyclic and monotonic behavior of all materials are taken into account in calculation of plastic hinge length.

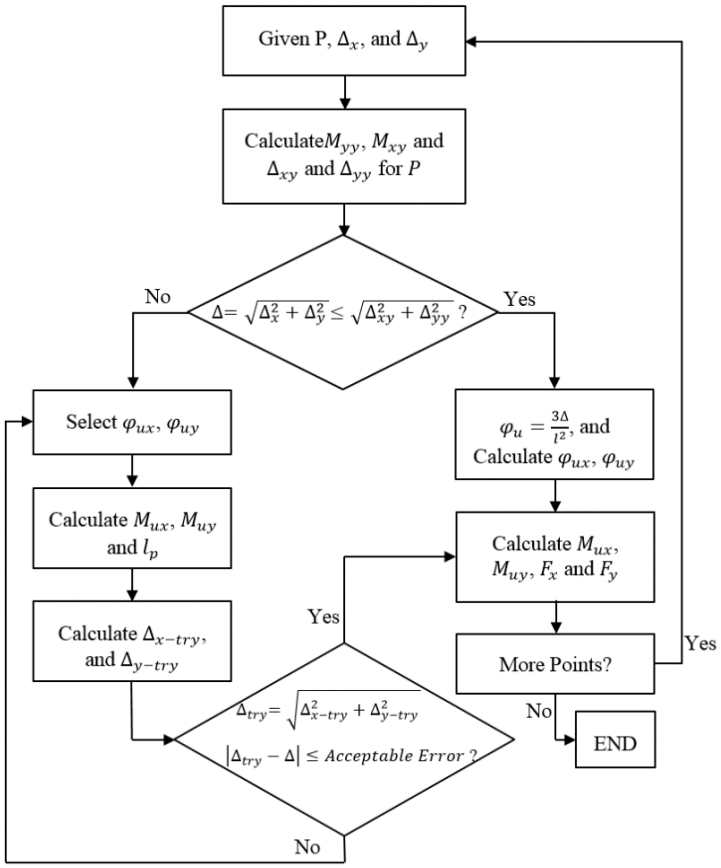

Fig. 11 Force-deflection analysis flowchart

Esmaeily's first plastic hinge length may increase by decreasing the ratio of yield moment to moment of critical section. It should be noted that plastic hinge length simulates the severe damage at column footing; thus, it cannot be decreased after formation (Esmaeily and Xiao 2002).

In Esmaeily's second plastic hinge method, the transition zone is divided into two parts. The curvature distribution along the closer part to the critical section is assumed to be uniform. The length of this part is constant and equal to the section depth for columns with a high to depth ratio of less than 12.5; otherwise, it is equal to 0.08×L where L is the column height. The curvature distribution along the second part is assumed to be linear and its length depends of the existing axial force and lateral force. Esmaeily's first and second methods yield more accurate results compared to the Priestley and Park and Priestley and Park-Revised by Xiao methods for RC columns under variable axial force and cyclic lateral force/displacement (Esmaeily and Xiao 2002). The curvature distribution along the column height as assumed in the aforesaid methods, is shown in Fig. 10 and their formulation is summarized in Table 3.

The developed computer application is also capable of conducting bi-axial force-deflection analysis. The axial load and lateral forces/displacements are applied at the top of column. For each combination of axial force and lateral displacement in the "x" and "y-direction" using two sets of iterations for D, φ_x and φ_y, axial force and lateral displacements are set to the applied values. The

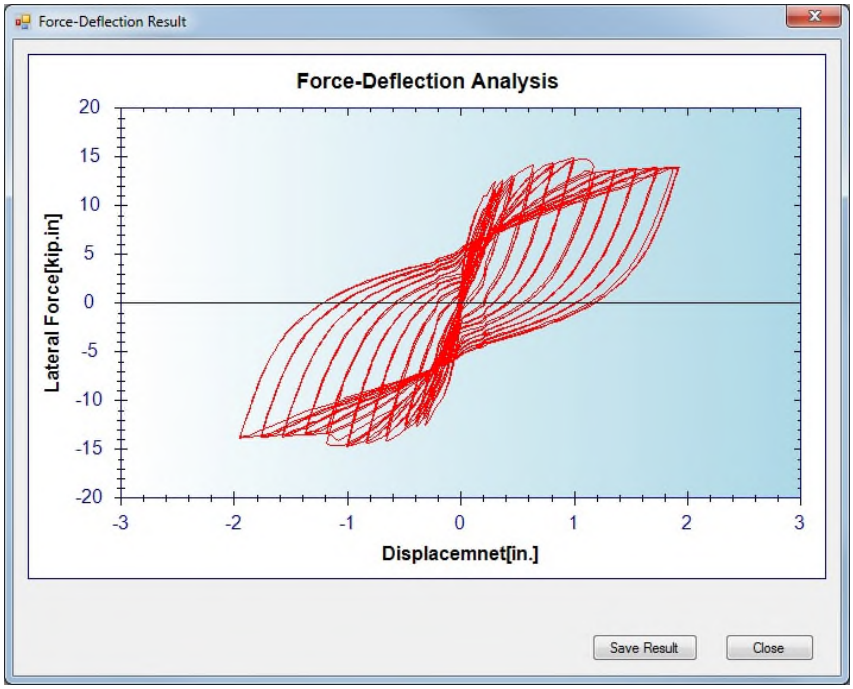

Fig. 12 Sample output form of force-deflection analysis

force-deflection analysis of a section under constant or variable axial force and cyclic or monotonic lateral displacement can be conducted using the aforesaid plastic hinge models implemented in the developed computer application. A simplified flowchart for force-deflection analysis of a RC column under axial force and bi-axial lateral displacement is shown in Fig. 11. Fig. 12 shows a sample output form of the developed windows-based computer application for force-deflection analysis.

5.3 Axial force-bending moment interaction surface

Three types of axial force-moment interaction 3D surface of a reinforced concrete section can be conducted using the developed computer program. In the first type, called as code-based axial force-moment interaction 3D surface, axial force-moment analysis is performed considering the ACI stress-block concept without considering the confinement effect applied by the lateral reinforcement. Compressive strain in the extreme concrete fiber is assumed to be equal to 0.003. Considering a specific angle for neutral axis with respect to the x-axis, for each level of axial force through an iteration process, curvature along the neutral axis is changed to converge to a curvature resulting in the considered axial force. When curvature is changed, the strain at the global coordinate's centroid is changed to keep the strain at the extreme compressive concrete fiber equal to 0.003. The code-based axial force-moment analysis can be performed only for concrete sections reinforced laterally by lateral steel reinforcement and longitudinally by steel bars.

The second type of axial force-moment interaction surface is calculated considering material models selected by user for plain concrete, confined concrete, reinforcing steel and FRP. This type of interaction surface can be calculated for concrete section confined by conventional steel

(a) (b)

Fig. 13 (a) Sinusoidal, (b) Triangular axial force loading pattern

(tie/spiral), FRP wraps or both FRP wraps and conventional steel. Strain at the extreme compressive fibers is assumed to be constant and can be defined by user.

The third type of interaction 3-D surface was called axial force-bending moment interaction failure surface in the literature. In the literature, four techniques have been employed to construct the 3-D failure surface of a composite section: (i) interaction curve considering constant or variable ratio of curvature along x- and y-axis (constant neutral axis orientation), (ii) interaction curve for a given ratio of bending moment in x- and y-direction, (iii) bending moment constant for a constant given axial force, and (iv) generation of triplets stress resultant extending an oriented strength line (Charalampakis and Koumousis 2008). The first technique (constant neutral axis orientation) was utilized in the developed computer application.

In various algorithms developed by researchers to calculate failure surface, the ultimate moment capacity of an RC section is defined as the maximum moment in monotonic moment-curvature analysis considering constant axial force (not considering the loading pattern of axial force). However, columns exposed to a dynamic excitation are subjected to a loading pattern in combined, but non-proportional lateral and axial directions. The importance of considering the axial force loading pattern when calculating bending capacity of an RC section is more pronounced in columns of structures located in near-fault regions (Saadeghvaziri and Foutch 1991, Lee *et al.* 2009, Shirmohammadi 2015).

The developed computer application is capable of generating the failure surface of a composite section using proper material models with or without considering the axial force loading pattern. To calculate the failure surface of a section while considering the axial force loading pattern for a specific neutral axis orientation and axial force level (P), a moment-curvature analysis is performed considering the pattern of axial force against curvatures along x- and y-directions, and the maximum moment was selected as the ultimate capacity of the section in that level of axial force. The axial force loading pattern includes a number of points with various curvature along the x- and y-axis and axial force coefficient (φ_x, φ_y, ac). The axial force coefficient (ac) for any combination of x- and y- curvature cannot exceed 1.0, meaning that the maximum compressive axial force ($ac \times P$) in that pattern is equal to the specified level of axial force (P). The axial force coefficient may consider more than -0.1, meaning that the maximum tensile axial force capacity of the section should not be considered more than $0.1 \times P$. A sinusoidal and triangular axial force loading patterns are shown in Fig. 13.

6. Validations examples

In this section the performance and applicability of the developed computer application are

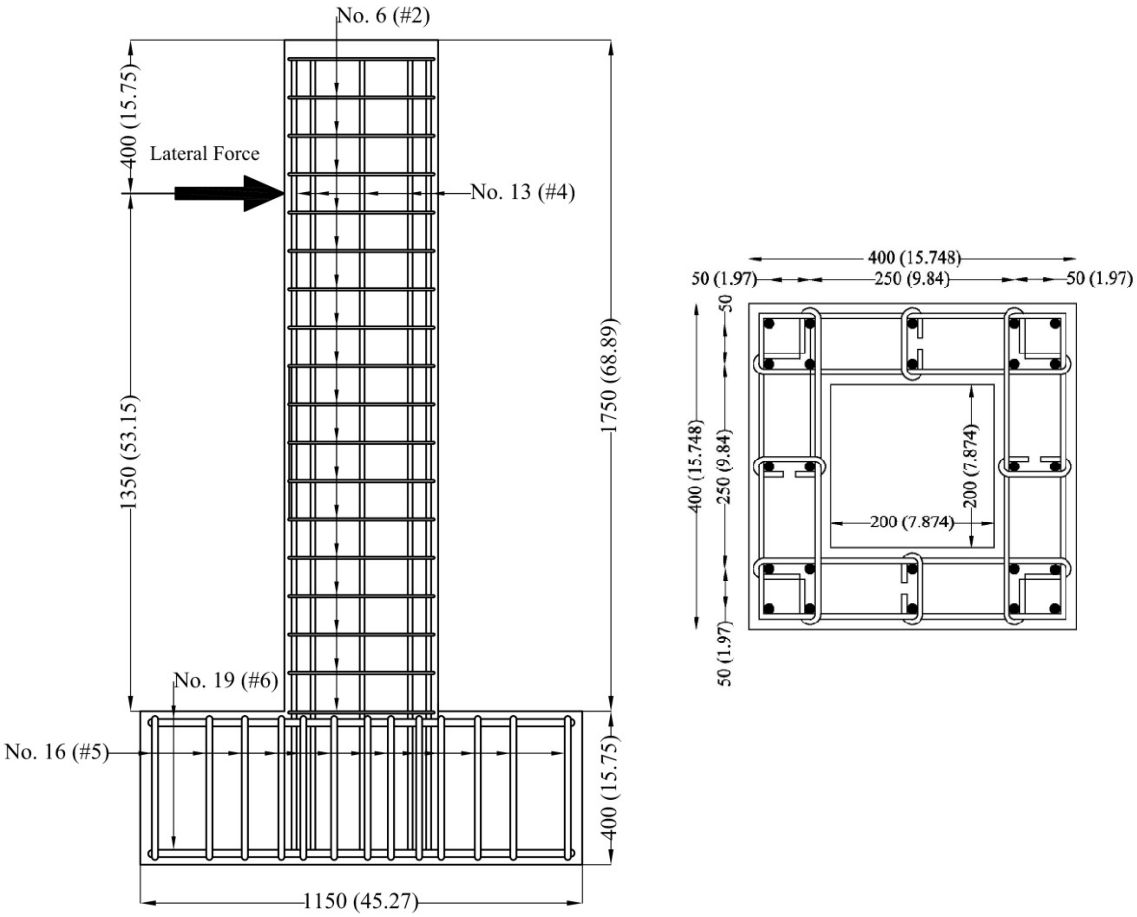

(a) (b)

Fig. 14 Geometry and reinforcement of the specimen TP-36; (a) Elevation, (b) Cross-section

presented through four examples, in which the analytical results by the program are compared to the experimental results from tests conducted on the respected specimen. The first example investigates the accuracy of the computer application to predict the moment-curvature response of a reinforced concrete section. In the second and third validation examples, the performance of the computer application in predicting the force-deflection response of two columns with their respected cross-sections is illustrated. Finally, the fourth test investigates the capability of the computer application in constructing the failure surface of a square section as well as the interaction curves using the ACI stress-block concept.

6.1 Moment-curvature analysis

The developed windows-based computer application was employed to conduct the moment-curvature analysis of a hollow square cross-section. The hollow square section, as shown in Fig. 14 has width of 400 mm (15.748 in.), cover width of 50 mm (1.97 in.), and hole width of 200 mm (7.874 in.). Cylinder strength of concrete was 29.7 MPa (4.05 ksi). The column specimen was

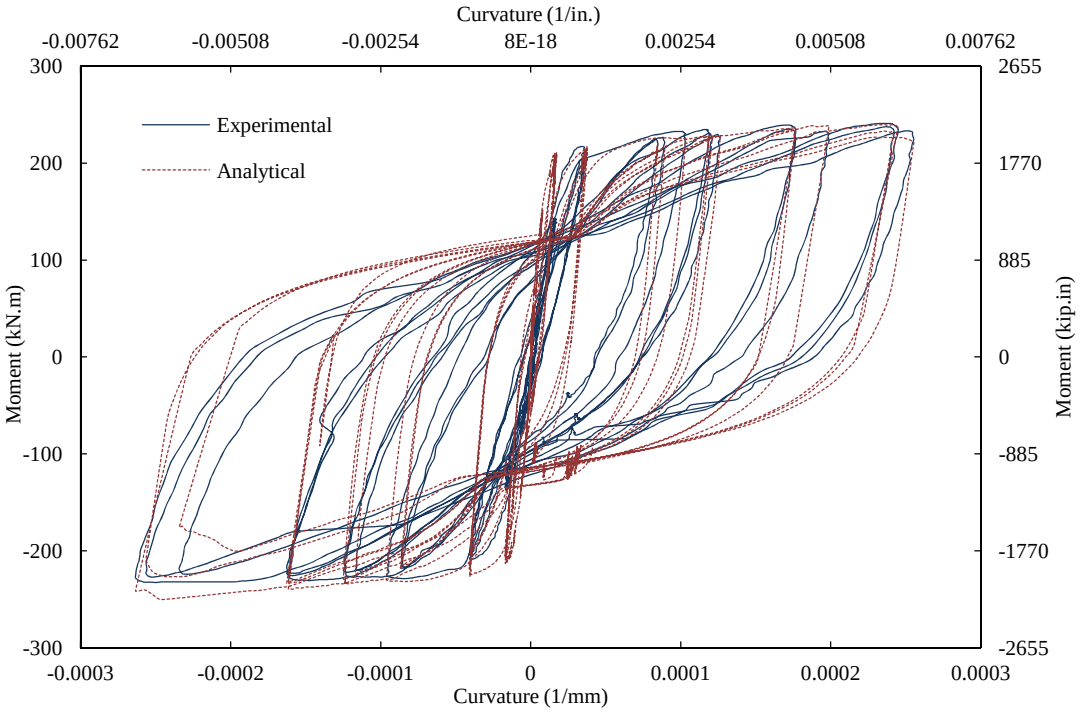

Fig. 15 Comparison of analytical and experimental moment-curvature response curves for the hollow square cross-section (TP-36)

reinforced longitudinally with 24 No. 13 (24 #4) Grade SD295A (yield strength was 374 MPa (54.24 ksi)), giving the specimen a longitudinal ratio of 2.53%. The longitudinal steel rebar arrangement is shown in Fig. 14. The transverse reinforcing steel was Grade SD295A with yield strength of 363 MPa (52.64 ksi). The lateral reinforcement was a No. 6 (#2) with a center-to-center spacing of 100 mm (3.93 in.), giving the specimen volumetric lateral reinforcement of 1.23%.

The column specimen was tested under constant axial force of 230 kN (51.71 kips) and cyclic uniaxial lateral force. The bending moment and curvature were measured at the column footing. Additional details regarding experimental setup are presented in Ref. (Kawashima *et al.* 2001).

To model the monotonic behavior of concrete fibers located in the cover and core concrete, the Mander *et al.* model (1988) for unconfined and confined concrete was employed, respectively. Mander *et al.*'s model was developed for circular and rectangular cross-sections without a hole/opening. To use this model to simulate monotonic behavior of confined concrete in a rectangular section with a hole/opening, an equivalent rectangular section without an opening was considered. Dimensions of the equivalent rectangular section were similar to the original section; however, only the outer layer of longitudinal and lateral reinforcement original section were considered as longitudinal and lateral reinforcement of equivalent section. The maximum strength, ultimate strain, and fracture strain of confined concrete in the hollow rectangular section was calculated considering the equivalent rectangular section in Mander *et al.*'s model (1988). The tensile strength for confined and unconfined concrete was assumed to be 10% of the plain concrete compressive strength. Linear cyclic behavior with a slope of plain concrete modulus of elasticity was considered for unconfined and confined concrete fibers.

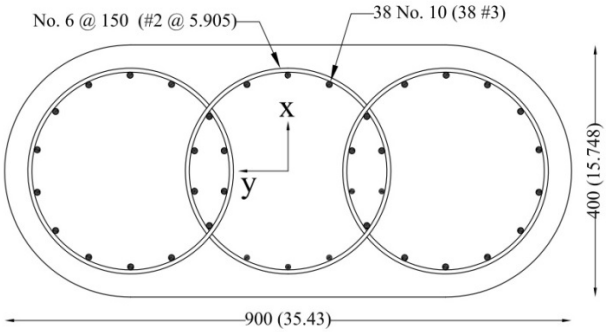

Fig. 16 Oval cross-section (TP-9)

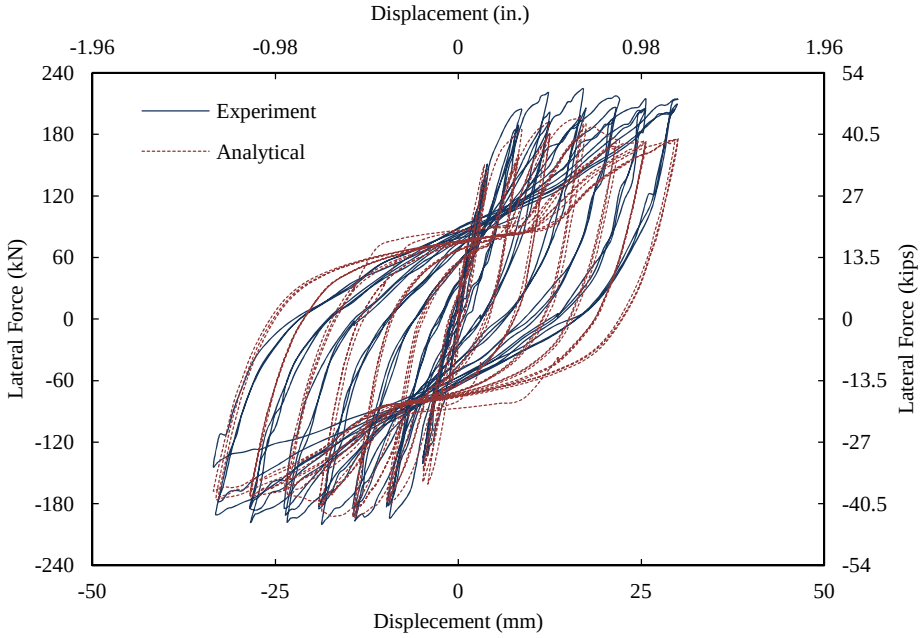

Fig. 17 Comparison of analytical and experimental force-deflection response curves for oval section

To model the cyclic and monotonic behavior of longitudinal steel bars, the Menegotto-Pinto's model (1973) was used. The monotonic curve backbone coefficient (*b*) in Menegotto-Pinto's model was set to 0.01. Cyclic parameters R_0, a_1 and a_2 were considered 2.0, 2.0, and 0.09, respectively.

Experimental and calculated moment-curvature curves at the bottom of the column specimen are shown in Fig. 15. As demonstrated in the figure, great agreement exists between experimental data and analytical results calculated by the developed windows-based computer application.

6.2 Force-deflection analysis

6.2.1 Reinforced concrete section under axial force and uniaxial lateral force

The developed fiber-based computer application was employed for force-deflection analysis of

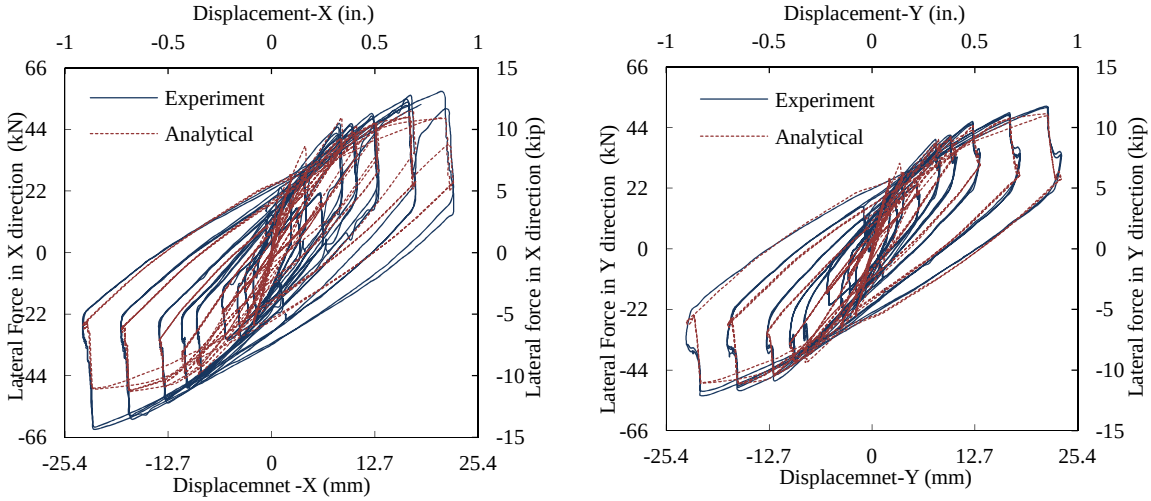

(a) (b)

Fig. 18 Comparison of analytical force-deflection with experimental data for specimen PB12-N15 in (a) x-, and (b) y-direction under expanding square path (Shirmohammadi and Esmaeily 2015)

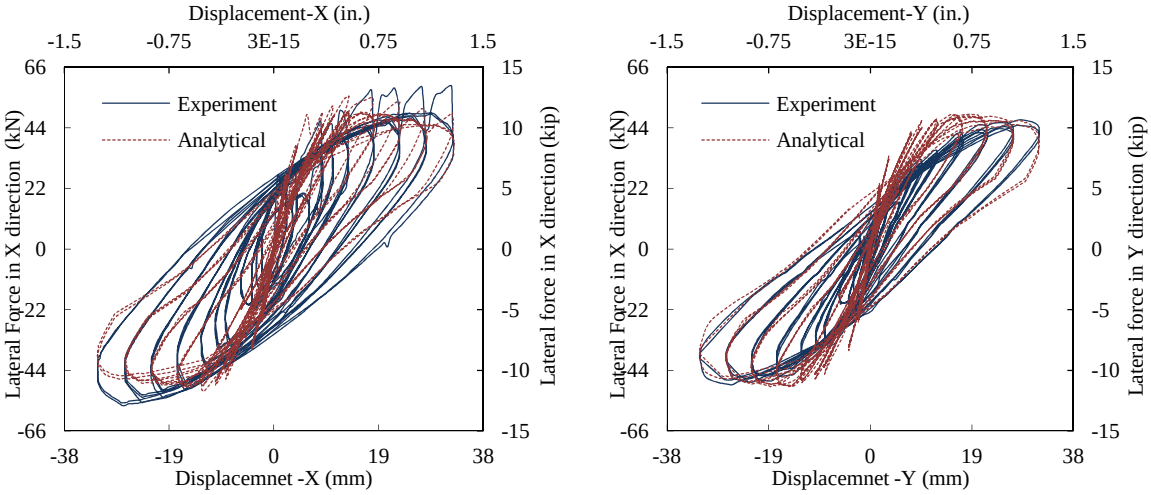

(a) (b)

Fig. 19 Comparison of analytical force-deflection with experimental data for specimens PB12-N16 in (a) x-, and (b) y-direction under expanding circular path (Shirmohammadi and Esmaeily 2015)

an oval section (TP-9) under constant axial force and uniaxial cyclic lateral force, tested by Fujikura *et al.* (1998). Geometrical properties of the oval section are shown in Fig. 16 in SI and imperial systems (numbers in parenthesis are in the imperial system). The column specimen was reinforced longitudinally with 38 No. 10 (38 #3) Grade SD295, giving the specimen a longitudinal ratio of 0.83%. The longitudinal steel rebar arrangement is shown in Fig. 16. The lateral reinforcement was provided using No. 6 (#2) with a center-to-center spacing of 150 mm (5.905

in.), giving the specimen volumetric lateral reinforcement of 0.9%. The cylinder strength of concrete ($f_c'_0$) was 22.7 MPa (3.292 ksi) and the yield strength of longitudinal and lateral steel was 379 MPa (54.97 ksi) and 380 MPa (55.114 ksi), respectively. This oval section was under constant axial force of 160 kN (35. 97 kips) and lateral uniaxial force in x-direction. Additional details regarding experimental setup are presented in Fujikura *et al.* (1998).

To model the behavior of confined concrete, Mander *et al.*'s model and linear cyclic model were used as monotonic and cyclic rules, respectively. The ultimate strain and stress and fracture strain of confined concrete in oval section were calculated considering only one of the circular hoop in the oval section as an equivalent section. Diameter of the equivalent cross section is equal to width of oval section (400 mm (15.748 in.)) and it is reinforced longitudinally and laterally using 14 No. 10 (14 #3) and No. 6 @ 150 mm (#2 @ 5.905 in.).

For plain concrete (located at the cover), Mander *et al.*'s monotonic model and linear cyclic model were employed. The Menegotto-Pinto monotonic and cyclic models modeled the behavior of longitudinal reinforcement. The monotonic curve backbone coefficient (*b*) in Menegotto-Pinto's model was set to 0.01. Cyclic parameters R_0, a_1 and a_2 were considered 2.0, 2.0, and 0.09, respectively. Esmaeily's first plastic hinge method (Esmaeily and Xiao 2005) was employed as curvature distribution along the specimen height. As shown in Fig. 17, fiber-based analysis was able to predict cyclic force-deflection of the oval section with reasonable accuracy.

6.2.2 Reinforced concrete section under axial force and bi-axial lateral forces

The second example of force-deflection analysis is related to bi-axial analysis of specimens PB12-N15 and PB12-N16 from Rodrigues *et al.*'s (Rodrigues *et al.* 2012) experimental work. In Rodrigues *et al.* (2012) experimental studies, specimens PB12-N15 and PB12-N16 were tested under expanding square and circular displacement paths, respectively, and constant axial force at approximately 10% of their theoretical axial capacity (theoretical axial capacity of an RC section is equal to $P_0=A_g\times f_c'_0$, where P_0, $f_c'_0$ and A_g are theoretical axial capacity, plain concrete compressive strength, and gross cross-section area, respectively). These two specimens had a square cross-section with dimension of 300 mm (11.81 ksi) and were reinforced longitudinally using eight No. 12 bars in European standard (No. 12 bar diameter is 12 mm (0.472 in.)), giving the specimen a longitudinal ratio of 1.01%. Lateral reinforcement was provided by No. 6 bars in European standard with a step of 150 mm (5.9 in.) (No. 6 bar diameter is 6 mm (0.236 in.)), giving the specimen volumetric lateral reinforcement of 0.21%. The cylinder strength of concrete ($f_c'_0$) was 21.57 MPa (3.13 ksi). The steel reinforcement grade in the longitudinal and lateral direction was A400NR-SD (European standard).

Monotonic behavior of longitudinal bars was modeled using an idealized bi-linear model. Since, no information was available about the monotonic curve of reinforcing steel material, as recommended by Esmaeily and Xiao (2002), the ultimate strain (ε_{su}) and strength (f_{su}) for steel was considered to be $24.9\times\varepsilon_{sy}$ and $1.3\times f_{sy}$, respectively. The linear model was used to model cyclic behavior of longitudinal bars with linear unloading-reloading stiffness.

For confined and unconfined concrete fibers, Mander *et al.*'s model (1988) for confined and unconfined concrete was used, respectively. Cyclic behavior of concrete fibers was considered linear with a slope equal to the modulus of elasticity of plain concrete. Priestly and Park plastic hinge method (1987) was employed as curvature distribution along the specimen height.

Experimental and analytical force-deflection curves of specimens PB12-N15 and PB12-N16 are shown in Fig. 18, and Fig. 19, respectively. As demonstrated in these figures, predicted results are in good agreement with experimental data.

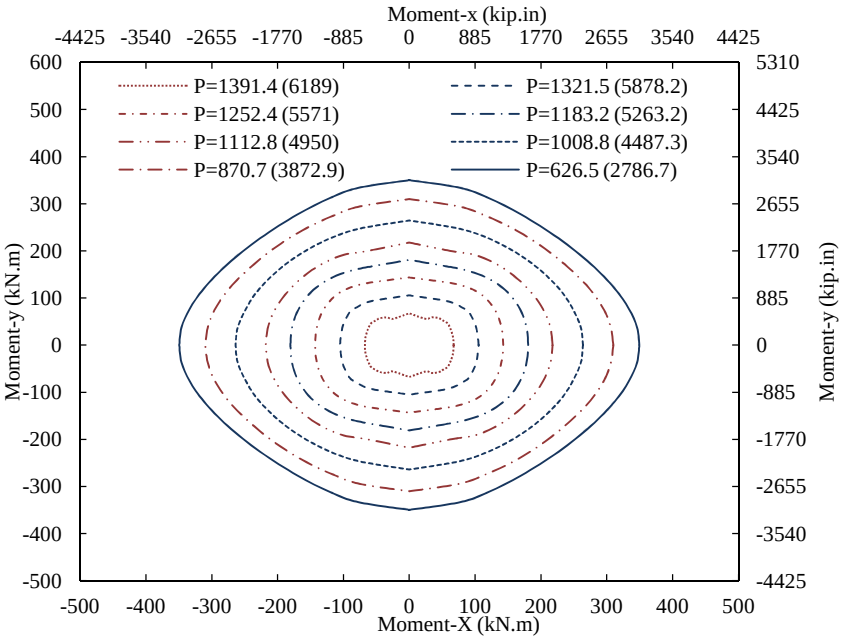

Fig. 20 Failure curves for square section

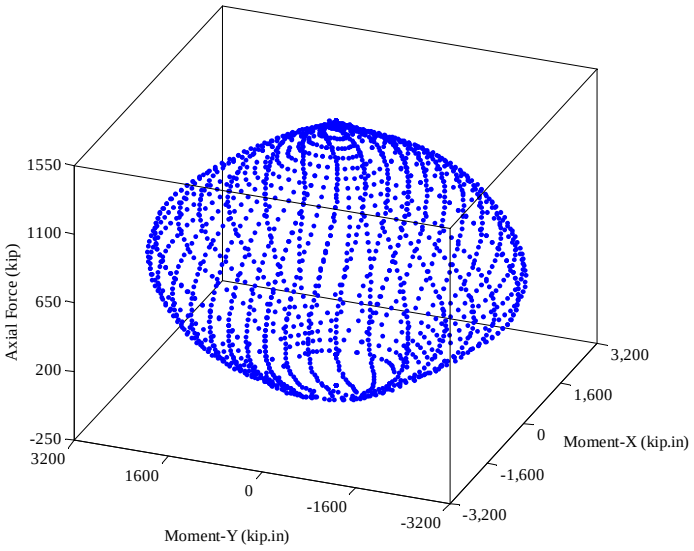

Fig. 21 Failure-surface of square section

6.3 Axial force-bending moment interaction curves

The axial force-bending moment failure surface was constructed for a square cross-section beam-column specimen with a dimension of 400 mm (15.75 in.). The square cross-section was

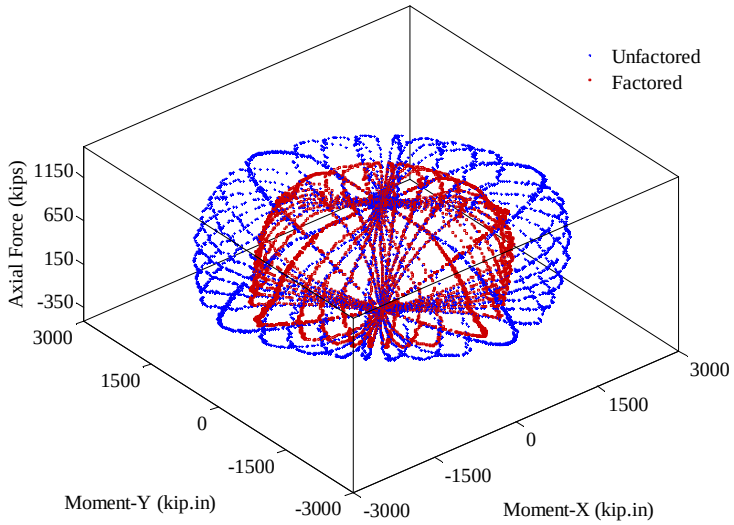

Fig. 22 Axial force-bending moment interaction surface

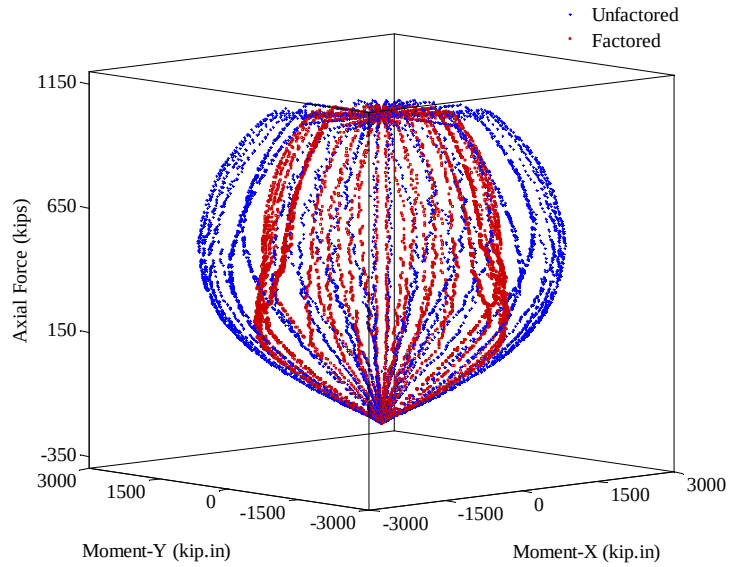

Fig. 23 Axial force-bending moment interaction surface

reinforced longitudinally using 20 No. 13 (20 #4), giving the specimen a longitudinal ratio of 1.58%. Lateral reinforcement was provided by No. 6 (#2) steel rebar with lateral spacing of 70 mm (2.75 in.), giving the specimen volumetric lateral reinforcement of 0.57. Cylinder strength of concrete was 35.9 MPa (5.207 ksi) and yield strength of longitudinal and lateral steel was 363 MPa (52.65 ksi) and 368 MPa (53.37 ksi), respectively.

The actual interaction curves and failure surface of the square section are demonstrated in Fig.

20 and Fig. 21, respectively. To construct these plots, Mander *et al.*'s confined and unconfined concrete models were used to model the behavior of confined and unconfined concrete fibers. The Menegotto-Pinto model was applied in order to model cyclic and monotonic behavior of longitudinal steel bars. Monotonic (b) and cyclic coefficients (R_0, a_1, a_2) in Menegotto-Pinto's model were considered 0.01, 2.0, 2.0, and 0.09, respectively.

In addition to actual failure surface, the axial force-bending moment interaction 3D surface of the square section was calculated considering the ACI-stress block method (ACI 318-11). In Fig. 22 and Fig. 23, the red and blue dots are related to the ACI-interaction surface with consideration of reduction factors and ACI-interaction surface without reduction factors.

7. Conclusions

A windows-based computer application was developed to analyze the behavior of RC columns subjected to various loading scenarios using fiber-based method. A number of monotonic material models and cyclic (hysteresis) rules for stress-strain relationship of the material, developed by the authors and adopted from the literature were implemented in the computer application. Since the developed computer application utilizes triangular meshing, column's cross-section can have any arbitrary shape. Monotonic and cyclic rules of materials can be unconditionally complex. The developed windows-based computer application can be used for:

• Construction of 3D axial force-bending moment interaction surface for RC columns with conventional lateral steel reinforcement using the American Concrete Institute (ACI) stress-block (code-based),

• Construction of axial force-bending moment interaction surface using proper material models for RC columns laterally reinforced by steel, FRP or steel and FRP assuming constant strain at extreme compressive fiber,

• Construction of real axial force-bending moment failure surface considering proper material models for RC columns laterally reinforced by steel, FRP or steel and FRP with or without considering the axial force loading pattern. The ultimate moment capacity of an RC section is defined as the maximum moment in monotonic moment-curvature analysis with constant or variable axial force,

• Moment-curvature analysis for RC columns with conventional lateral steel reinforcement considering ACI stress-block (code-based),

• Biaxial moment-curvature analysis considering proper material models under any pattern of curvature in the two lateral directions and arbitrary axial load pattern,

• Biaxial force-deflection analysis using proper material models and plastic hinge method under any pattern of lateral displacement in the two lateral directions and an arbitrary axial load pattern.

The accuracy of calculated results by the developed computer application was assessed through some validation examples in which the analytical predictions were compared to the experimental results. The calculated results show a close agreement with the experimental data. The effect of loading pattern of axial and lateral forces in the two lateral directions on the response of concrete columns confined by conventional lateral steel reinforcement or FRP or both lateral steel and FRP can be captured using proper monotonic and cyclic material models and assumption on curvature distribution along the column height. In addition, the accuracy of the existing monotonic and cyclic material models and curvature distribution assumption (plastic hinges methods) can be assessed through various types of analysis when the experimental data is available.

References

American Concrete Institute 318 (2011), Building Code Requirements for Reinforced Concrete and Commentary, American Concrete Institute, Farmington Hills, Michigan.

Bonet, J.L., Romero, M., Miguel, P.F. and Fernandez, M.A. (2004), "A fast stress integration algorithm for reinforced concrete sections with axial loads and biaxial bending", *Comput. Struct.*, **82**(2-3), 213-225.

Charalampakis, A.E. and Koumousis, V.K. (2008), "Ultimate strength analysis of composite sections under biaxial bending and axial load", *Adv. Eng. Softw.*, **39**(11), 923-936.

Codeplex. Triangle. Accessed (2014), http://triangle.codeplex.com/.

Cusson, D. and Paultre, P. (1995), "Stress-strain model for confined high-strength concrete", *J. Struct. Eng.*, **121**(3), 468-477.

Esmaeily, A. and Xiao, Y. (2002), "Seismic behavior of bridge columns subjected to various loading ratterns", Report PEER 15/08, Pacific Earthquake Engineering Research Center, College of Engineering, University of California.

Esmaeily, A. and Xiao, Y. (2005), "Behavior of reinforced concrete columns under variable axial loads: analysis", *ACI Struct. J.*, **102**(5), 736-744.

Esmaeily, A. and Peterman, R.J. (2007), "Performance analysis tool for reinforced concrete members", *Comput. Concrete*, **4**(5), 331-346.

Esmaeily, A. and Shirmohammadi, F. (2014), "Performance and capacity assessment of reinforced concrete bridge piers considering the current load and resistance factor design provisions and plastic hinge length in Kansas, K-TRAN: KSU-11-5.

Fafitis, A. (1985), "Lateral reinforcement for high-strength concrete columns", *J. ACI*, **87**, 213-232.

Fafitis, A. (2000), "Interaction surfaces of reinforced concrete sections in biaxial bending by Green's Theorem", *Comput. Civil Build. Eng.*, 90-97.

Fujikura, S., Kawashima, K., Shoji, G., Zhang, J. and Takemura, H. (1998), "Strength and ductility of reinforced concrete bridge columns with interlocking ties and cross ties", Report No. TIT/EERG 98-9, Tokyo Institute of Technology, Tokyo, Japan.

Hoshikuma, K., Kawashima, K., Nagaya, K. and Taylor, A.W. (1997), "Stress-strain model for confined reinforced concrete in bridge piers", *J. Struct. Eng.*, **123**(5), 624-633.

Hostani, M., Kawashima, K. and Hoshikuma, J. (1998), "A stress-strain model for concrete cylinders confined by both carbon fiber sheets", *J. Concrete Eng.*, **39**(592), 37-52.

Kawashima, K., Hostani, M. and Yoneda, K. (2000), "Carbon fiber sheet retrofit of reinforced concrete bridge piers", *Proceedings of the International Workshop on Annual Commemoration of Chi-Chi Earthquake*, Vol. II-Technical Aspect, National Center for Research on Earthquake Engineering, Taipei, Taiwan, ROC, 124-135.

Kawashima, K., Une, H. and Sakai, J. (2001), "Seismic performance of hollow reinforced concrete arch ribs subjected to cyclic lateral force under varying axial load", Report No. TIT/EERG 01-1, Tokyo Institute of Technology, Tokyo, Japan.

Lam, L. and Teng, J.G. (2003), "Design-oriented stress-strain model for FRP-confined concrete", *Constr. Build. Mater.*, **17**(6-7), 471-489.

Lee, J.Y., Yi, C.K., Jeong, H.S., Kim, S.W. and Kim, J.K. (2009), "Compressive response of concrete confined with steel spirals and FRP composites", *J. Compos. Mater.*, **44**(4), 1-24.

Mander, J.B., Priestley, M.J.N. and Park, R. (1984), "Seismic design of bridge piers", Research Report No. 84-2, University of Canterbury, New Zealand.

Mander, J.B., Priestley, M.J.N. and Park, R. (1988), "Theoretical stress-strain model for confined concrete", *J. Struct. Eng.*, **114**(8), 1804-1826.

Marante, M.E. and Flórez-López, J. (2002), "Model of damage for RC elements subjected to biaxial bending", *Eng. Struct.*, **24**, 1141-1152.

Mazzoni, S., McKenna, F. and Fenves, G.L. (2006), "Open system for earthquake engineering simulation user manual", Pacific Earthquake Engineering Research Center, University of California, Berkeley.

Menegotto, M. and Pinto, P. (1973), "Method of analysis for cyclically loaded reinforced concrete plane

frames including changes in geometry and non-elastic behavior of elements under combined normal force and bending", *Proceedings of IABSE Symposium on Resistance and Ultimate Deformability of Structures Acted on by Well Defined Repeated Loads*, International Association for Bridge and Strcutural Engineering, Zurich, Switzerland.

Papanikolaou, V.K. (2012), "Analysis of arbitrary composite sections in biaxial bending and axial load", C*omput. Struct*, **98-99**, 33-54.

Popovics, S. (1973), "A numerical approach to the complete stress-strain curve of concrete columns", *Cement Concrete Res.*, **3**(5), 583-599.

Prakash, V., Powell, G. and Campbell, S. (1987), "DRAIN-2DX base program description and user guide", Rep. No. UCB/SEMM-93/17, Dept. of Civil Eng., University of California, Berkeley.

Priestley, M.J.N. and Park, R. (1987), "Strength and ductility of concrete bridge columns under seismic loading", *ACI Struct. J.*, **84**(1), 61-76.

Richard, R.M. and Abbott, B.J. (1975), "Versatile elastic-plastic stress-strain formula", *J. Eng. Mech.*, **101** (4), 511-515.

Rodrigues, H., Arede, A., Varum, H. and Costa, A.G. (2012), "Experimental evaluation of rectangular reinforced concrete column behavior under biaxial cyclic loading", *Earthq. Eng. Struct. Dy.*, **42**(2), 239-259.

Rodrigues, H., Varum, H., Arede, A. and Costa, A.G. (2013), "Behavior of reinforced concrete columns under biaxil cyclic loading-state of the art", *Int. J. Adv. Struct. Eng.*, **5**(1), 1-12.

Rodriguez, J.A. and Aristizabal-Ochao, J.D. (1999), "Biaxial intraction diagrams for short RC columns of any cross section", *J. Struct. Eng.*, **125**(6), 672-683.

Rosati, L., Marmo, F. and Serpieri, R. (2008), "Enhanced solution strategies for the ultimate strength analysis of composite steel-concrete sections subject to axial force and biaxial bending", *Comput. Method. Appl. Mech. Eng.*, **197**(9-12), 1033-1055.

Samaan, M., Mirmiran, A. and Shahawy, M. (1998), "Model of concrete confined by fiber composites", *J. Struct. Eng.*, **124**(9), 1025-1031.

Saadeghvaziri, M.A. and Foutch, D.A. (1991), "Dynamic behavior of R/C highway bridges under the combined effect of vertical and horizontal earthquake motions", *J. Earthq. Eng. Struct. Dyn.*, **20**(6), 535-549.

Sfakianakis, M.G. (2002), "Biaxial bending with axial force of reinforced, composite and repaired concrete sections of arbitrary shape by fiber model and computer graphics", *Adv. Eng. Softw.*, **33**(4), 227-242.

Shirmohammadi, F., Esmaeily, A. and Kiaeipour, Z. (2014), "Stress-strain model for circular concrete columns confined by FRP and conventional lateral reinforcement", *Eng. Struct.*, **84**, 395-405.

Shirmohammadi, F. and Esmaeily, A. (2015), "Performance of reinforced concrete columns under bi-axial lateral force/displacement and axial load", *Eng. Struct.*, **99**, 63-77.

Shirmohammadi, F. (2015), "Effect of load pattern and history on performance of reinforced concrete columns", Diss. Kansas State University.

Sousa, B.M. and Muniz, C.F.D.G. (2007), "Analytical integration of cross section properties for numerical analysis of reinforced concrete, steel and composite frames", *Eng. Struct.*, **29**(4), 618-625.

Thorenfeldt, E., Tomaszewicz, A. and Jensen, J.J. (1987), "Mechanical properties of high-strength concrete and application in design", *Proceedings of the Symposium on Utilization of High Strength Concrete*, Tapir, Trondheimr, Norway, 149-159.

Yau, C.Y., Chan, S.L. and So, A.K.W. (1993), "Biaxial bending design of arbitrary shaped reinforced concrete column", *ACI Struct. J.*, **90**(3), 269-278.

Yen, J.Y.R. (1991), "Quasi-newton method for reinforced concrete column analysis and design", *J. Struct. Eng.*, **117**(3), 657-666.

Youssef, M.N., Feng, M.Q. and Mosallam, A.S. (2007), "Stress-strain model for concrete confined by FRP composites", *Compos.: Part B*, **38**(5-6), 614-628.

Notations

A= cross-section area

A_{ci} = area of i^{th} concrete fiber

A_{fi} = area of i^{th} FRP fiber

A_g =gross cross-sectional area

A_{shx} = total cross-sectional area of transverse bars perpendicular to x-axis

A_{shy} = total cross-sectional area of transverse bars perpendicular to y-axis

A_{si} = area of i^{th} steel bar

A_{sp} = area of transverse reinforcement bar

a_1 = Menegotto-Pinto cyclic model first coefficient

a_2 = Menegotto-Pinto cyclic model second coefficient

b =Menegotto-Pinto monotonic backbone coefficient

b_c = width of core concrete between tie for rectangular section

c_x = side dimension of concrete core parallel to x-axis

c_y = side dimension of concrete core parallel to y-axis

d = diameter of circular column

D = strain at the global coordinate's centroid

d_c = diameter of core concrete between tie or spiral bar for circular section and height of core concrete between tie for rectangular section

E_1 =initial stiffness in stress-strain model

E_2 =secondary stiffness in stress-strain model

E_c = modulus elasticity of concrete

E_{frp} = modulus of elasticity of FRP

$E_{\sec}$ = tangent modulus of elasticity of the concrete

f_c = axial stress in concrete

$f_{c0}^{'}$ = maximum axial compressive strength of unconfined concrete

$f_{cc}^{'}$ = compressive strength of confined concrete

f_{cu} = axial stress in concrete corresponding to complete formation of failure plane

f_{cs} = compressive stress of confined concrete at yielding of steel spiral

f_{hcc} = stress in transverse reinforcement steel at the maximum strength of confined concrete

$f_l^{'}$ = effective lateral confining pressure

f_{lf} = normal lateral pressure caused by FRP reinforcement

f_{ls} = normal lateral pressure caused by transverse steel reinforcement applied to the concrete core

f_{sy} =yield strength of steel material

f_{su} =ultimate (maximum) strength of steel material

f_t = axial stress at the boundary point of the first and second region in which the jacket begins to be fully activated in Youssef et al.'s model

f_0 = intercept or reference stress in axial direction

f_{yh} = yield strength of transverse reinforcement

F_x = lateral force in x-direction

F_y = lateral force in y-direction

k_1= stress coefficient, which is a function of concrete mix and lateral pressure caused by transverse reinforcement

k_2 = strain coefficient, which is a function of concrete mix and lateral pressure caused by transverse reinforcement

K_1 to K_4 =parameters for monotonic stress-strain relationship of steel in Esmaeily-Xiao's model

k_e = effective lateral confining coefficient

k_s = transverse steel reinforcement confinement coefficient

$M_{cr-after}$ = bending moment right after developing first crack in concrete

$M_{cr-before}$ = bending moment right before developing first crack in concrete

M_x = bending moment along x-axis

M_{xy} = yield moment along x-axis

M_y = bending moment along y-axis

M_{yy} =yield moment along y-axis

M_{ux} =moment at critical section along x-axis

M_{uy} =moment at critical section along y-axis

n= curve-shape parameter in axial direction

n_c = number of concrete fibers

n_f = number of FRP fibers

n_s = number of steel bars

P= applied axial force

P_0 = theoretical axial capacity of a section

P_1 to P_3 =parameters in hysteretic stress-strain model of steel (for stress level)

r = ratio of modulus of elasticity

R_0 = Menegotto-Pinto cyclic model coefficient

R_1 and R_2 =parameters in hysteretic stress-strain model of steel (for stiffness change)

s = center-to-center spacing or pitch of spiral or circular hoop

s' = clear spacing of circular hoop, spiral, or rectangular tie

t = total thickness of FRP wraps

w_i' = i^{th} clear distance between adjacent longitudinal bars

$\overline{x}$ = centroid of cross-section with respect to the x-axis of global coordinate

x_{ci} = location of i^{th} concrete fiber with respect to global y-axis

x_{fi} = location of i^{th} FRP fiber with respect to global y-axis

x_{si} = location of i^{th} steel bar with respect to global x-axis

$\overline{y}$ = centroid of cross-section with respect to the y-axis of global coordinate

y_{ci} = location of i^{th} concrete fiber with respect to global y-axis

y_{fi} = location of i^{th} FRP fiber with respect to global y-axis

y_{si} = location of i^{th} steel bar with respect to global y-axis

ε_c = axial strain in concrete

ε_{C50U} = strain at which the stress drops to 50% of the peak strength of unconfined concrete

ε_{C50C} = strain at which the stress drops to 50% of the peak strength of confined concrete

ε_{cc} = corresponding strain of maximum stress of confined concrete

ε_{ci} = axial strain at i^{th} concrete fiber

ε_{ci}^{p} = previous axial strain of i^{th} concrete fiber

ε_{c0} = axial strain in unconfined concrete corresponding to $f_{c0}^{'}$

ε_{cs} = compressive strain of confined concrete at yielding of steel spiral

ε_{cu} =ultimate strength of confined concrete

ε_{fi} = axial strain at i^{th} FRP fiber

ε_{fi}^{p} = previous axial strain of i^{th} FRP fiber

ε_{frp} = tensile rupture strain of FRP

ε_{jt} = FRP jacket strain at transition from first to second region in Youssef et al.'s model

ε_{RO} = strain of the last point reached in unloading branch

ε_{si} = axial strain at i^{th} steel bar

ε_{si}^{p} = previous axial strain of i^{th} steel bar

ε_{sy} =yield strain of steel material

ε_{su} =ultimate strain of steel material

ε_t = axial strain at the boundary point of the first and second region in which jacket begins to be fully activated in Youssef et al.'s model

ε_{un} = strain of the last point reached on the monotonic model

σ = axial stress

σ_{ci} = axial stress of i^{th} FRP concrete

σ_{ci}^{p} = previous axial stress of i^{th} concrete fiber

σ_{fi} = axial stress of i^{th} FRP fiber

σ_{fi}^{p} = previous axial stress of i^{th} FRP fiber

σ_{RO} = stress of the last point reached in unloading branch

σ_s =stress of steel

σ_{si} = axial stress of i^{th} steel bar

σ_{si}^{p} = previous axial stress of i^{th} steel bar

σ_{un} = stress of the last point reached on the monotonic model

ρ_s = ratio of the volume of transverse confining steel to the volume of confined concrete core

ρ_{cc} = ratio of area of longitudinal reinforcement to area of core of section

φ_{cr} =curvature when first crack develops in concrete

φ_u = curvature at critical section

φ_{ux} = curvature at critical section along x-axis

φ_{uy} = curvature at critical section along y-axis

φ_x = curvature along x-axis

φ_y = curvature along y-axis

Δ =total displacement

Δ_x =displacement in x-direction

Δ_{x-try} =trial displacement in x-direction

Δ_{xy} =yield displacement in x-direction

Δ_{try} =trial total displacement

Δ_y =displacement in y-direction

Δ_{y-try} = trial displacement in y-direction

Δ_{yy} = yield displacement in y-direction